Journal of Wind Engineering & Industrial Aerodynamics 213 (2021) 104611

Contents lists available at ScienceDirect

Journal of Wind Engineering & Industrial Aerodynamics

journal homepage: www.elsevier.com/locate/jweia

An analysis of historical wind-driven rain loads for selected Canadian cities

Zhe Xiao [a,b,*], Michael A. Lacasse [a], Elena Dragomirescu [b]

[a] National Research Council Canada, Institute for Research in Construction, Ottawa, ON, Canada
[b] University of Ottawa - Civil Engineering Department, Ottawa, ON, Canada

ARTICLE INFO

Keywords:
Wind-driven rain
Climate loads
Extreme value analysis
Goodness of fit test

ABSTRACT

The performance and durability of wall assemblies are greatly affected by the moisture load to which they may be subjected, in particular those arising from Wind-Driven Rain (WDR). Standard approaches for estimating such moisture loads assume 1% of the WDR load, whereas these loads have also been assessed from watertightness tests, although these assumed loads have been determined based on limited climate information. To more accurately estimate the moisture loads to which wall assemblies may be subjected over their service life, an analysis of historical WDR loads was completed for 11 cities across Canada. The magnitude, probability of occurrence of WDR loads in different cities and correlations between WDR related climate parameters, are discussed in this paper. Also, a novel WDR severity index is introduced, referred to as the Wind-Driven Rain Pressure Index, to permit quantifying the real-time and simultaneously occurring effects of WDR intensity and Driving Rain Wind Pressure (DRWP). To estimate the WDR intensity and DRWP with a specific probability of occurrence, an Extreme Value Analysis (EVA) was completed for a climate dataset of 31 years (1986–2016) using the Generalized Extreme Value and Gumbel distributions.

1. Introduction

The long-term performance and durability of building façades, for which the façade maintains the function and integrity of a structure by impeding most of the detrimental effects of the surrounding environment from entering the building envelop, are adversely affected by moisture loads to which they may be subjected over time (Desjarlais et al., 2001; Rousseau, 1999; Smegal et al., 2013). For example, in respect to masonry walls, mould growth problems may arise at the interior layers of the wall assembly due to excessive moisture load (Abuku et al., 2009b). For wood-framed wall assemblies, the wood materials can decay when exposed to a humid environment for prolonged periods of time (Chouinard and Lawton, 2001). Other undesirable problems arising from the presence of moisture in masonry and cementitious wall clad assemblies include, but are not limited to, frost damage of, and salt migration in porous materials, the erosion of building materials and efflorescence at the surface of the façades (Charola and Lazzarini, 1986; Franke et al., 1998; Tang et al., 2004; Van Balen, 1996).

Wind-driven rain (WDR), as the primary source of the moisture load for wall assemblies, is the co-occurrence of wind and rain (Lacy, 1977). The horizontal velocity component of raindrops, as part of WDR, can be attributed to the action of wind and its direction usually in accordance with the wind velocity vector. The amount of water that is deposited on a vertical surface of a building façade is identified as the WDR load, which can be assessed by semi-empirical equations provided the rainfall intensity, wind velocity and direction, and the surrounding conditions are known (ASHRAE, 2016; ISO, 2009; Lacy, 1977; Straube and Burnett, 2000). A more accurate assessment for WDR load at specific locations may require the information of building geometry (Blocken et al., 2009; Blocken and Carmeliet, 2006; Karagiozis et al., 1997; Kubilay et al., 2015). In addition, the WDR load on a building façade can also be determined from field measurements by installing collection troughs at exterior surfaces of the façade (Blocken and Carmeliet, 2005; Ge et al, 2017, 2018; Kubilay et al., 2014; Wang et al., 2020).

When a raindrop reaches the façade of a building, it may splash, spread, or bounce from the building surface, depending on the façade materials, on the raindrop final velocity, as well as on the attack angle between the raindrop and the wall assembly (Abuku et al., 2009a). After the impact, the raindrop would either be drained from the façade, absorbed by façade materials, provided theses are porous in nature, or enter the building envelop through any deficiencies, such as cracks or openings present on the façade surface. However, the existence of deficiencies in the building envelop also allows the passage of water through these openings, over its life cycle, and this is most likely

* Corresponding author. National Research Council Canada, Institute for Research in Construction, M24, 1200 Montreal Road, Ottawa, ON, Canada.
E-mail addresses: zxiao014@uottawa.ca (Z. Xiao), Michael.Lacasse@nrc-cnrc.gc.ca (M.A. Lacasse), Elena.Dragomirescu@uottawa.ca (E. Dragomirescu).

https://doi.org/10.1016/j.jweia.2021.104611
Received 12 October 2020; Received in revised form 22 March 2021; Accepted 22 March 2021
Available online xxxx

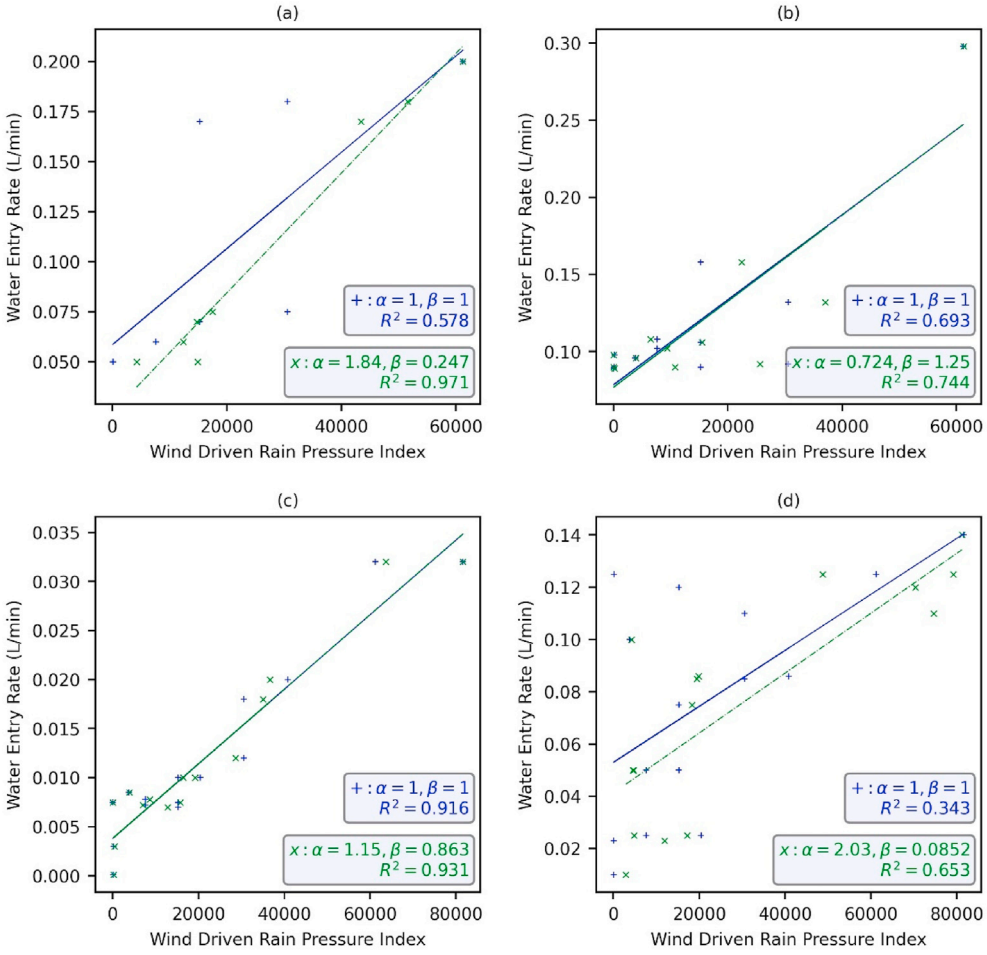

Fig. 1. (a) Stucco wall assembly (WA-4)* - Water entry rate at deficiency above electrical outlet; (b) EIFS wall assembly (WA-7)* - Water entry rate at vertical joint; (c) Hardboard siding wall assembly (WA-16)* - Water entry rate at the ventilation duct; (d) Hardboard siding wall assembly (WA-16)* - Water entry rate at the window. * **Designations of wall assemblies from the MEWS project** (Lacasse et al., 2003).

Table 1
Frequency of rain events and ratio of averaged annual maximum wind velocity and wind pressure during rain events to that for all hours.

City	Rain Frequency %	Wind Velocity %	Wind Pressure %
Calgary	3.15	76.1	59.4
Charlottetown	6.3	81.9	68.4
Halifax	7.74	91.2	83.9
Moncton	6.2	82.1	68.8
Montreal	9.69	83.3	70.3
Ottawa	6.01	81.5	67.7
Saskatoon	3.92	87.3	77.7
St. Johns	7.63	82.2	68.9
Toronto	7.49	84.2	72.1
Vancouver	19.8	91.1	83.8
Winnipeg	4.1	85.2	73.8

inevitable given the effect of aging and deterioration of materials, mechanical failure of structural members arising from extreme and cyclic loads and faulty construction and maintenance practice. Currently, there are two typical approaches to quantify the amount of water, namely the moisture load, that could penetrate the exterior cladding of the wall assembly during WDR events. One approach is to simply consider that the moisture load is 1% of the WDR load to which the exterior wall surface is subjected during a rain event, as specified in the ASHRAE standard 160 (ASHRAE, 2016). Another approach is to conduct a watertightness test in which water spray onto the wall assembly and pressure difference across the wall are applied simultaneously to simulate the action of WDR on the wall test specimen. Such tests are able to quantify the rate of water entry across the exterior wall cladding and the portion of water that enters the wall assembly (Boardman and Glass, 2013; Bossche et al., 2012; Sahal and Lacasse, 2004, 2005).

The National Research Council Canada has launched a series of research studies the results of which have permitted establishing a watertightness test protocol to properly manage risks of damage to wall assemblies over the long-term due to moisture loads arising from WDR. As such, the entire assessment encompasses the following steps: (i) Understanding the WDR conditions based on climatic data collected at meteorological stations and from which to derive the WDR load; (ii) Measuring the level of water entry in and water retention of wall assemblies exposed to the corresponding WDR loads through watertightness tests using the new test protocol; (iii) Relating the climate data with the rate of water entry to wall assemblies; (iv) Correlating the degree of water retention with the moisture response of wall assemblies.

In this paper, the historical WDR conditions from 1986 to 2016 are analyzed for 11 cities located across Canada and the results are discussed at different temporal scales. Outputs from the analysis were used to determine boundary conditions for the new watertightness test protocol to be established using the information described in this paper.

2. Methodologies

2.1. Observational dataset

Hourly rainfall intensity and wind velocity for different cities were obtained from the climate dataset for 1986 to 2016, as recorded at

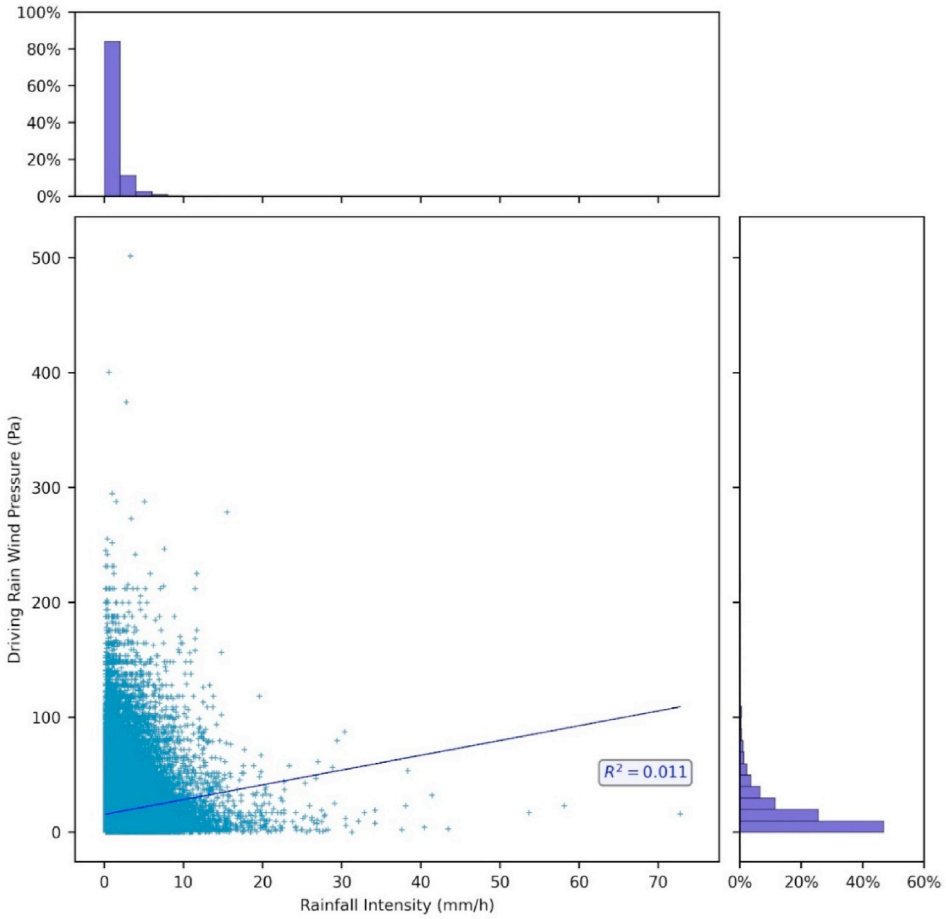

Fig. 2. Correlations and histograms between DRWP and concurrent rainfall intensities for all cities.

meteorological stations operated by Environment and Climate Change Canada. Rainfall is usually measured using a standard rain gauge consisting of a 40 cm high and 11.3 cm diameter cylindrical metal container, where the volume of collected rain water is funneled into a graduated cylinder for the measurement. Based on the hourly rate, the rainfall intensity is classified as "Very light", i.e., rain does not completely wet a surface; "Light" i.e., greater than a trace and up to 2.5 mm an hour; "Moderate", i.e., rate of rainfall is between 2.6 mm and 7.5 mm per hour, and; "Heavy", i.e., 7 mm per hour or more. Wind velocities and directions are measured by an anemometer placed at a height of 10 m. Precipitation events during hours of snowfall were also recorded and differentiated from those of rainfall; these data were excluded from the analysis in this study.

2.2. WDR and DRWP

The amount of water that is deposited on a vertical exterior wall surface during a rain event is defined as the WDR load to the wall. The semi-empirical equation used to calculate this load based on the rainfall intensity and the wind speed, was firstly proposed by Hoppestad (1955) and subsequently further developed and improved by Lacy (1977), and thereafter, Straube and Burnett (2000). The applicability and limitations of these equations have been discussed in detail by Blocken and Carmeliet (2004). Subsequent versions of equations used to calculate the WDR load, which were also put in practice for practical applications, were specified in ISO 15927 standard (ISO, 2009) and ASHREA standard 160 (ASHRAE, 2016). Eqs. (1) and (2) are the semi-empirical expressions used to calculate the WDR load, as given in the ISO15927 standard (ISO, 2009):

$$I_A = \frac{2}{9}\,\Sigma v R_h^{8/9}\cos(D-\theta) \tag{1}$$

$$I_{AW} = I_A C_R\, C_T O W \tag{2}$$

In which I_A is the airfield WDR index, v is the hourly mean wind speed (m/s) at the given height, R_h is the hourly rainfall intensity (mm/h), D is the angle between hourly wind speed directions and the north, and θ is the wall orientation in regard to the north direction.

To assess the WDR load (I_{WA}) on a building façade, a few more factors were considered in addition to the airfield WDR index, specifically the terrain roughness coefficient C_R, topography coefficient C_T, obstruction factor O and the wall factor W. These factors are individually determined for each case of interest.

Eq. (3) is the semi-empirical equation specified in the ASHRAE standard 160 (ASHRAE, 2016) to calculate the WDR load:

$$r_{bv} = r_h \mathrm{F_E F_D F_L} U cos\theta \tag{3}$$

where r_{bv} is the rain deposition rate on a vertical wall kg/(m^2·h), r_h is the rainfall intensity on a horizontal surface (mm/h), F_E is the rain exposure factor, F_D is the rain deposition factor, F_L is an empirical constant, 0.2 kg·s/(m^3·mm), U is the hourly average wind speed (m/s) and θ is the angle between the wind direction and normal to the wall. Amongst these factors, the rain exposure factor (F_E), the deposition factor (F_D), and the wind direction angle (θ) are determined considering the configurations of the building and the topography surrounding the building.

Both sets of equations consider the effect of wind direction, exposure of the wall, and surrounding topography for estimating the WDR load on a wall surface. The ISO 15927 standard considers the effect of a possible

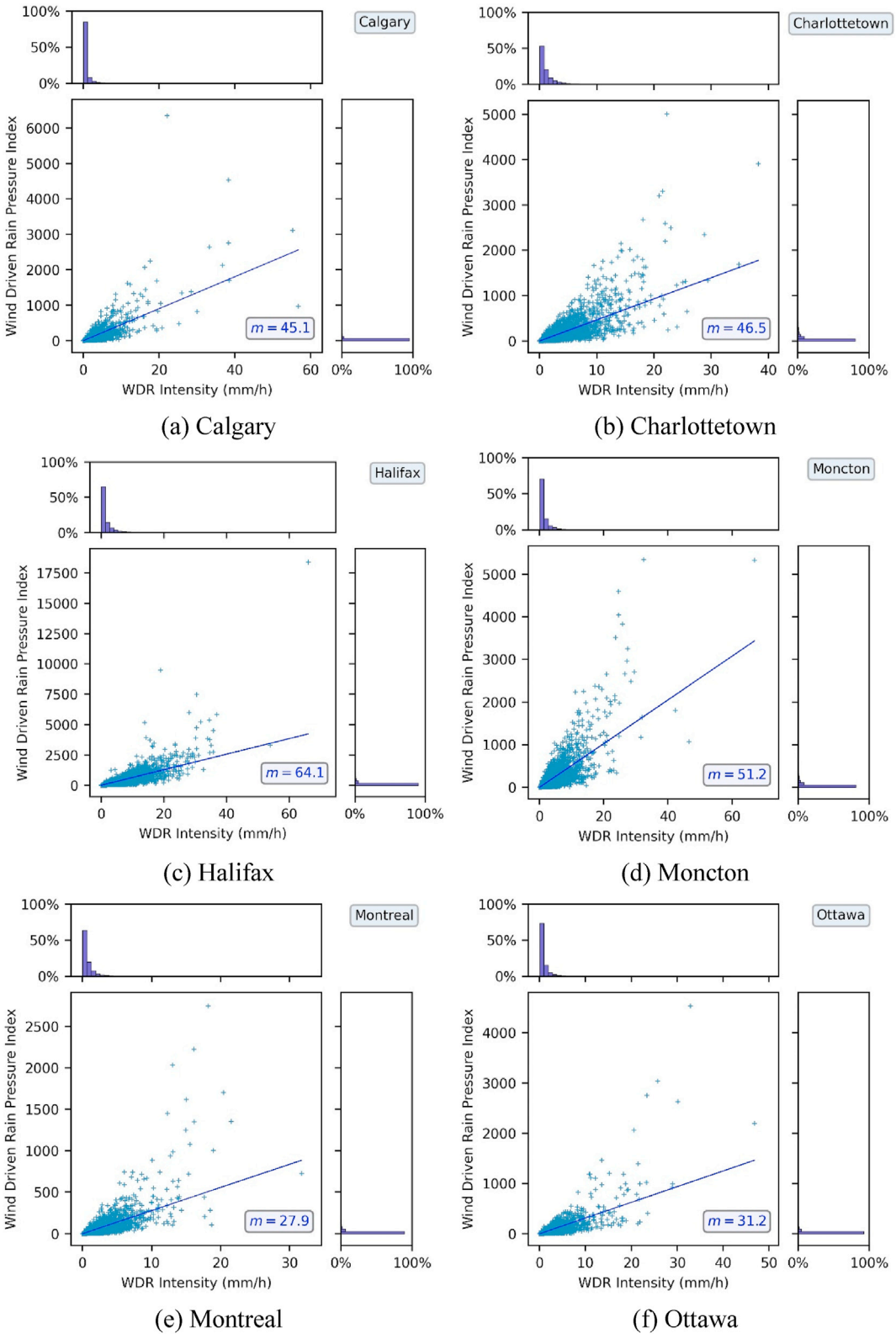

Fig. 3. The WDR intensity and WDRP index in different cities.

obstruction near the wall, which is ignored in the ASHREA standard. The wall factor *W* of the ISO 15927 standard describes the distributions of WDR load on wall assemblies for different types of building configurations without taking water runoff into account. Runoff on the wall surface is, however, considered in the ASHREA standard through the use of a rain deposition factor but this factor lacks accounting for the distribution of the WDR load in the horizontal direction.

The WDR load in this study was calculated using the semi-empirical equation provided in the ASHREA standard given that when undertaking a hygrothermal simulation, the WDR load is usually coupled with

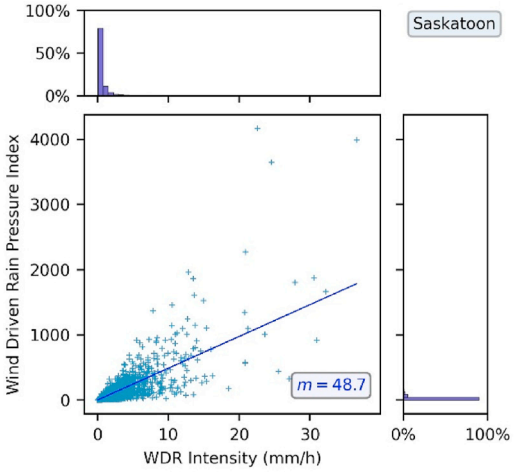

(g) Saskatoon

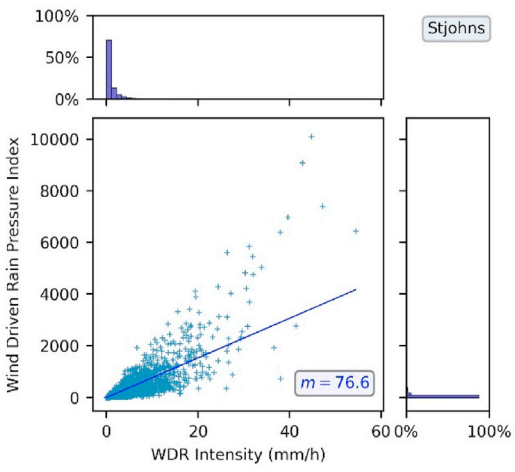

(h) St. Johns

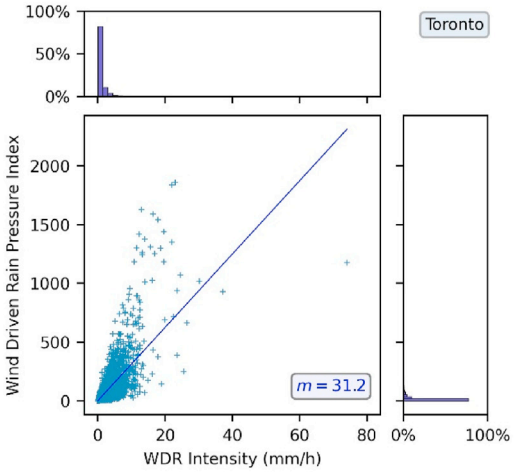

(i) Toronto

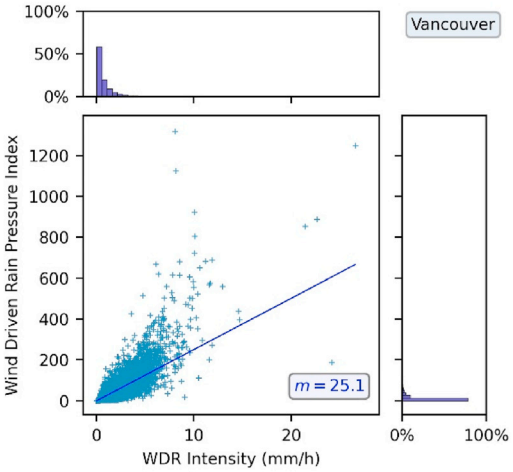

(j) Vancouver

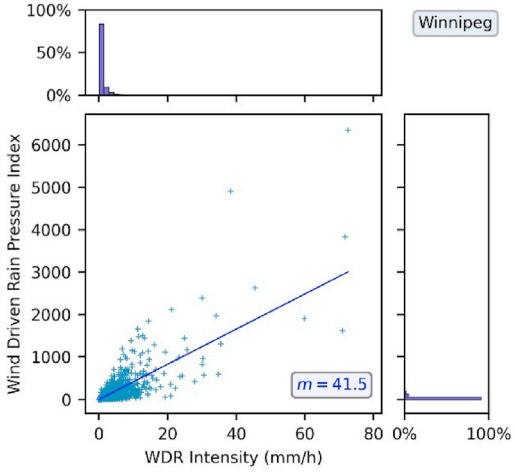

(k) Winnipeg

Fig. 3. (*continued*).

other criteria in the ASHREA standard pertinent to this use. To normalize the WDR analysis undertaken in this study, which is intended for the characterisation of WDR loads on buildings, the values of the rain exposure factor (F_E) and the deposition factor (F_D) were set to 1. The hourly horizontal rainfall intensity and hourly averaged wind velocity were the two primary climate variables considered, which could readily be obtained from the available climate data.

To permit simulating WDR effects on wall assemblies from a water-tightness test, water deposition onto the wall assembly and pressure differential across the assembly must be applied to a test specimen simultaneously, in controlled magnitudes, given that these parameters, represent, respectively, the WDR load and Driving Rain Wind Pressure (DRWP) as might be acting on a wall for a specified amount of time during a rain event. Regarding the applied pressure during testing, Mayo

Table 2
Cumulative probability of WDR and DRWP in different cities.

Cumulative Probability		0.5	0.9	0.95	0.99	0.995	1
Calgary	*WDR (mm/h)*	0.587	2.74	4.2	9.36	12.4	56.7
	DRWP (Pa)	10.7	37.1	51.5	91.5	109	288
Charlottetown	*WDR (mm/h)*	0.75	3.45	5.22	11	14	38.2
	DRWP (Pa)	17.1	46.9	64.7	100	118	225
Halifax	*WDR (mm/h)*	0.799	4.94	8.01	16	20.1	66.1
	DRWP (Pa)	13.1	53.9	72.8	109	124	501
Moncton	*WDR (mm/h)*	0.639	3.6	5.34	11.7	14.7	77
	DRWP (Pa)	13.6	48.4	64.7	109	128	231
Montreal	*WDR (mm/h)*	0.435	1.8	2.78	5.98	7.7	31.7
	DRWP (Pa)	6.23	22.9	29.5	50.4	60.2	156
Ottawa	*WDR (mm/h)*	0.54	2.3	3.54	7.94	10.9	46.8
	DRWP (Pa)	9.27	27.2	37.1	57.9	70	176
Saskatoon	*WDR (mm/h)*	0.542	2.42	3.73	8.96	12.2	36.6
	DRWP (Pa)	18.9	51.5	64.7	100	118	194
St. Johns	*WDR (mm/h)*	0.467	3.23	5.33	12.3	16.4	54.4
	DRWP (Pa)	7.98	51.5	73.2	128	148	288
Toronto	*WDR (mm/h)*	0.529	2.57	4	8.61	11.1	74.1
	DRWP (Pa)	11.1	35.3	47.4	76.8	88.8	202
Vancouver	*WDR (mm/h)*	0.44	1.93	2.78	5.06	6.04	26.6
	DRWP (Pa)	7.98	23.4	31.3	49.9	59.6	165
Winnipeg	*WDR (mm/h)*	0.5	2.38	3.83	9.74	13.1	72.6
	DRWP (Pa)	13.6	42.5	57.9	95.7	109	358

(1998) suggested that the most extreme wind pressure be used based on the longest period of time as recorded for the DRWP load. However, the most extreme wind pressure for all hours might not be representative of the level of wind pressure present during rain events. Sacré et al. (Sacré, 1984) and Surry et al. (1997) indicated that the peak wind velocities during rain events were 5%–30% lower when compare to those for all hours of wind and the corresponding peak wind pressure should be reduced by 10%–51%. Hourly wind velocities from the historical dataset for Canadian cities for all hours during rain events will be discussed in the subsequent section of this paper.

According to the results of multiple watertightness tests (Bossche et al., 2012; Sahal and Lacasse, 2004, 2005), water ingress to a wall assembly can be affected by both the water spray rate and concurrently applied pressure differential. Choi (1994) characterized the relationship between the wind and rain to permit calculating the driving rain from a driving-rain index. Cornick and Lacasse (2010) reported a poor correlation between the rainfall intensity and wind during rain events and a weak positive correlation between the WDR and DRWP, which was attributed likely to the WDR equation that included the DRWP as a factor. Van Den Bossche et al. (2013) developed a spectrum for the WDR and DRWP using a Pareto Front Analysis which provided boundary conditions of these two parameters for different return periods. Pérez-Bella et al. (2013) addressed a Risk Index for Water Penetration, as given in Eq. (4), that permits integrating both the WDR and DRWP parameters:

$$RIWP = \sqrt{\alpha \cdot (WDR)^2 + \beta \cdot (DRWP)^2} \tag{4}$$

In which, α and β were two weighting factors and the WDR and DRWP were normalised by the minimum and maximum values for 30 years of sample climate data. Although, from these studies it was possible to summarize the correlation and to quantify the two simultaneous factors over a long period of time, it was not possible to reflect the real-time WDR and DRWP conditions. Consequently, these relations could not be used to establish the relationship between the co-occurrence of WDR, DRWP and the water entry rate, which would be used in the subsequent hygrothermal simulations.

As a means of representing real-time WDR conditions to which a wall assembly may be exposed during rain events, a new Wind-Driven-Rain Pressure (*WDRP*) index, is proposed; this is the product of the *WDR intensity* (mm/h) and the simultaneous action of *DRWP* (Pa). The WDR intensity describes the amount of water that is deposited onto the exterior surface of the wall assembly and the pressure differences across the wall assembly derived from the DRWP, which induces the force that drives the water into the wall assembly when deficiencies are present. Although the response of the wall assemblies to WDR and DRWP are not the same due to many factors, such as the selection of wall components and materials, wall cavity depths, and the size of deficiencies, it is supposed that the value of the WDRP index may be determined as given in Eq. (5). The coefficients α and β would be applied to different configurations of wall assemblies according to the performance of the wall when subjected to watertightness tests.

$$WDRP = WDR^{\alpha} \cdot DRWP^{\beta} \tag{5}$$

Correlations between the WDRP index and the water entry rate obtained from the MEWS project (Lacasse et al., 2003) are shown in Fig. 1. The vertical axis of each plot is the water entry rate in L/min during a watertightness test and the horizontal axis is the corresponding WDRP index calculated from the experimental inputs of that test, i.e., the spray rate representing the WDR intensity and applied pressure as represented by the DRWP in Eq. (5). The blue '+' mark is the water entry rate (L/min) at a WDRP index that considers α and β equal to 1 and the green '**x**' mark represents the water entry rate (L/min) at a WDRP index calculated from flexible adjustment. The blue solid line and the green dotted line are the trendlines for each set of relations. It is evident that the correlations between the water entry rate and the WDRP index have increased by adjusting the two coefficients, α and β, for WDR intensity and DRWP respectively. The water entry rates at the deficiency above the electrical outlet for a stucco wall assembly, as shown in Fig. 1 (a), are more sensitive to the variation of WDR intensity than the variation of DRWP given α, the adjustment coefficient for WDR intensity, is larger than β, the adjustment coefficient for the DRWP. In contrast, the variation of water entry rates at the vertical joint for an EIFS wall assembly, as shown in Fig. 1 (b), is more greatly affected by the variation of the DRWP, as the value of β is larger than that of α. Fig. 1 (c) and 1(d) show the water entry rates for two different deficiencies in the same type of wall assembly. The water entry rates at the ventilation duct are not as greatly affected by the DRWP and more so by the WDR intensity, as compared to that for the water entry rates at the window given a smaller value of α and a larger value of β. When analyzing the WDRP index from the climate data, both coefficients are considered as having a value of 1.

2.3. Distributions for EVA

Extreme value distributions are usually applied to extreme events such as annual maximum rainfall and in hydrology, to river discharges rates to estimate the severity of these events at different return periods. The life span of wall assemblies is usually greater than 31 years, which is the length of collected historical climate data for this study. To evaluate the extreme WDR conditions for a longer period of time, Intensity-Duration-Frequency (IDF) curves were generated for different hourly values of WDR intensity and WDRP index. Empirical approaches (Chow, 1962; Sherman, 1931) were mostly implemented to generate IDF curves for the rainfall intensity with respect to hydraulic engineering applications. Within these approaches the values of parameters usually varied with location and the duration of rain events. In this study, the Gumbel distribution (Eq. (6)), Fréchet distribution (Eq. (7)), Weibull distribution (Eq. (8)), and Generalized Extreme Value (GEV) distribution (Eq. (9)) were selected to analyze the extreme values of WDR intensities and hourly WDRP index. The annual maximum values of WDR intensity and hourly WDRP index over different durations for 31 years have been selected to fit with these distributions. The value of the parameters of these distributions obtained from the fitting process would thereafter be used to calculate the WDR intensities and hourly WDRP indices at different return periods. Goodness of fit tests were also carried out to examine the effectiveness of the four distributions.

$$G_{(\mu,\sigma)}(x) = EXP\left(- (EXP)^{\frac{-(x-\mu)}{\sigma}} \right) \tag{6}$$

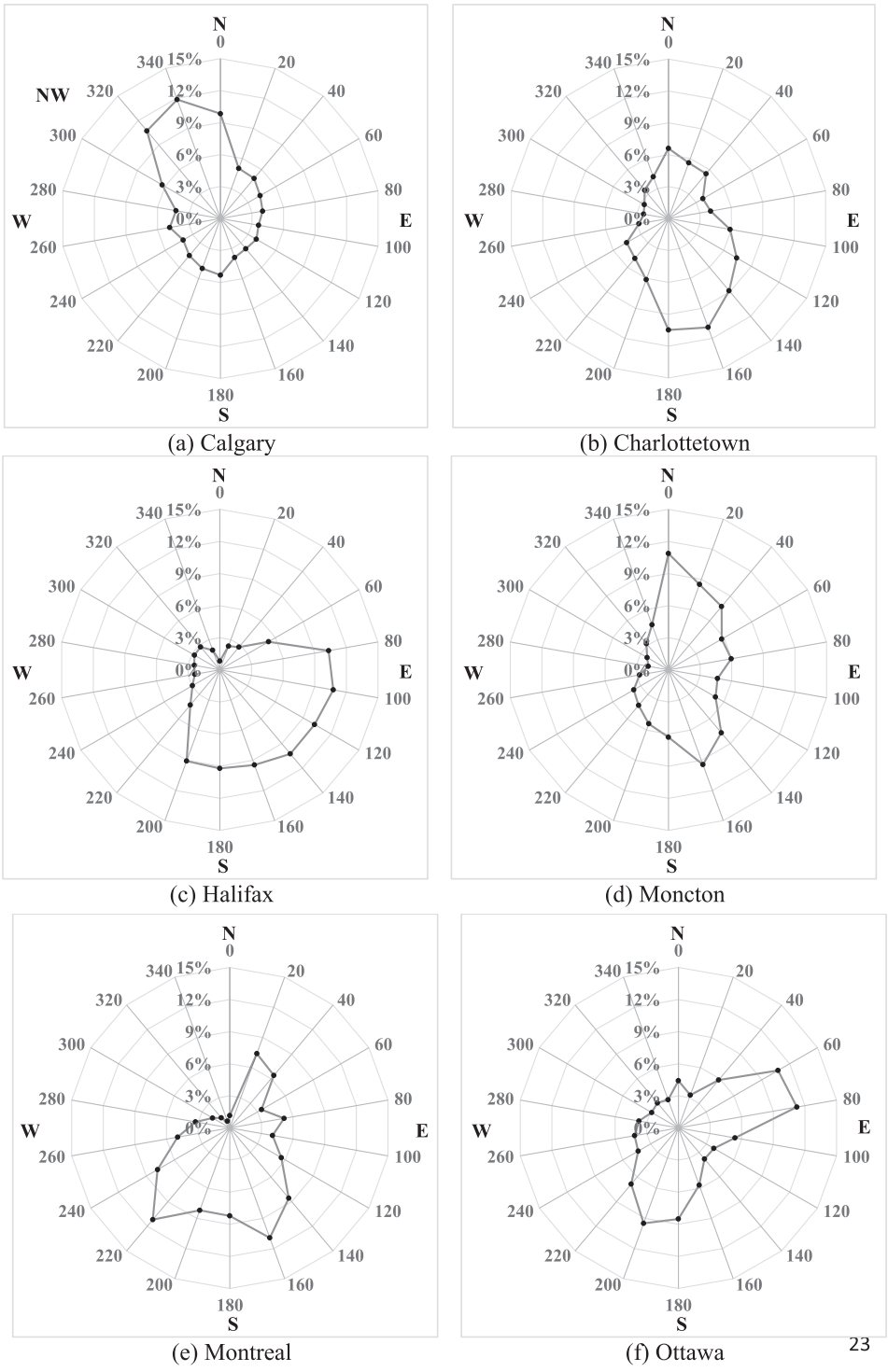

Fig. 4. Distributions of wind directions during rain events.

$$G_{(\xi,\mu,\sigma)}(x) = EXP\left(-\left(\frac{x-\mu}{\sigma}\right)^{-1/\xi}\right) \tag{7}$$

$$G_{(\xi,\sigma)}(x) = 1 - EXP\left(-\left(\frac{x}{\sigma}\right)^{\xi}\right) \tag{8}$$

$$G_{(\xi,\mu,\sigma)}(x) = EXP\left(-\left(1+\xi\left(\frac{x-\mu}{\sigma}\right)\right)^{-\frac{1}{\xi}}\right) \tag{9}$$

3. WDR conditions for selected cities

Parameters in the climate dataset that may affect the WDR load on a wall assembly include frequency of rain events, wind velocity during rain events, rainfall intensity, and direction of rain events. The frequency of rain events is representative of how often a wall assembly may be subjected to WDR and can be quantified by the number of rain hours in the climate dataset. This is an important factor to be considered when characterizing performance of wall assemblies used in different regions having different climatic conditions given that increases in the frequency

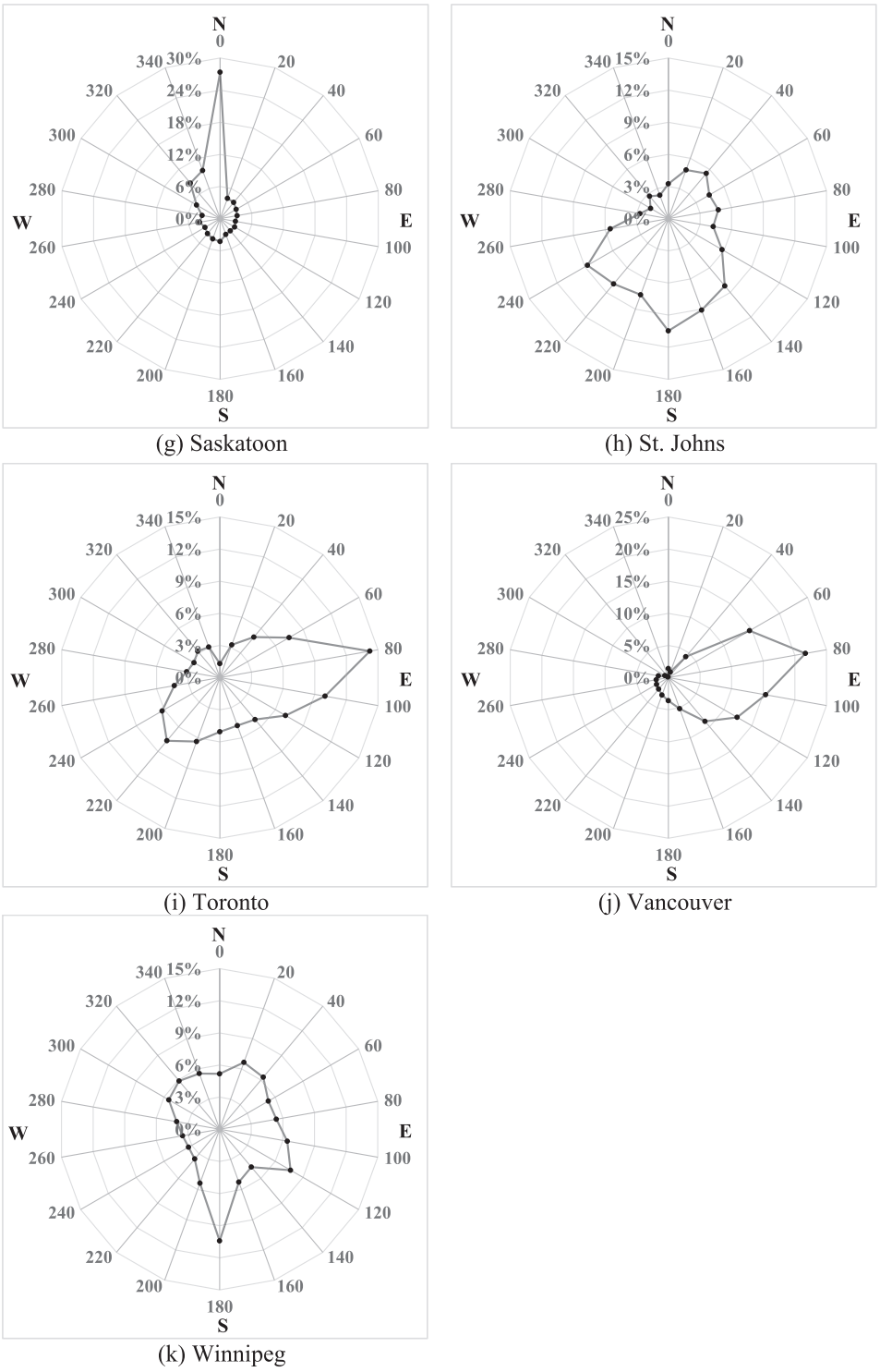

Fig. 4. (*continued*).

Table 3
Goodness of fit test scores.

Distributions	Chi-square test			BIC		
	WDR Scores	WDRPI Scores	Total Scores	WDR Scores	WDRPI Scores	Total Scores
Fréchet	20	24	44	19	24	43
Weibull	12	22	34	11	18	29
Gumbel	36	23	59	60	39	99
GEV	130	129	259	108	117	225

of rain events assuredly have an adverse effect on the long-term performance of wall assemblies. The wind velocity and rainfall intensity are the two primary parameters from which the WDR load is derived. Knowledge of the probability of occurrence and distribution of the magnitude of both these parameters permit understanding the differences of WDR conditions in distinct cities, as well as providing specific conditions to which a watertightness test could be conducted. The proposed WDRP index could reveal the relative severity amongst wind-driven rain events given the rainfall intensity and DRWP of an event. Since the product of the rainfall intensity and DRWP cannot be larger than the maximum value for the

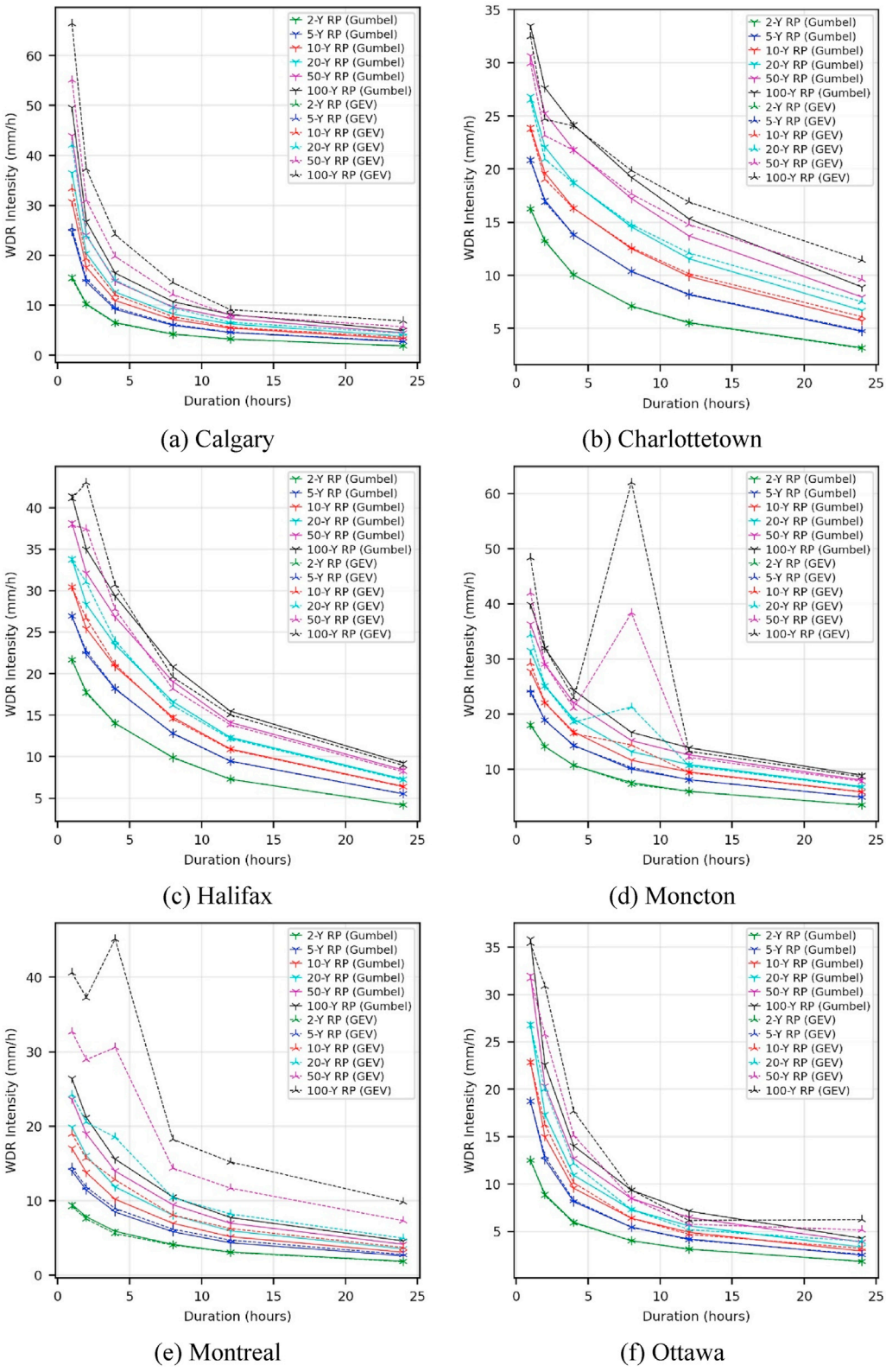

Fig. 5. IDF curves for WDR in each city investigated.

WDRP index, this then represents the extent of influence in respect to the risk of water entry of these climate load parameters when acting together. Knowing the prevailing wind direction in different cities will be helpful in determining the most problematic direction, in regards to the risk to water entry to which a wall assembly is exposed during a WDR event.

3.1. Rainfall and wind

Frequencies of rain events are depicted as the Rain Frequency (%) in Table 1. It is the ratio between the number of hours with rainfall to the total number of hours over a period of 31 years. For each city, the annual maximum hourly wind velocities during rain events were selected and

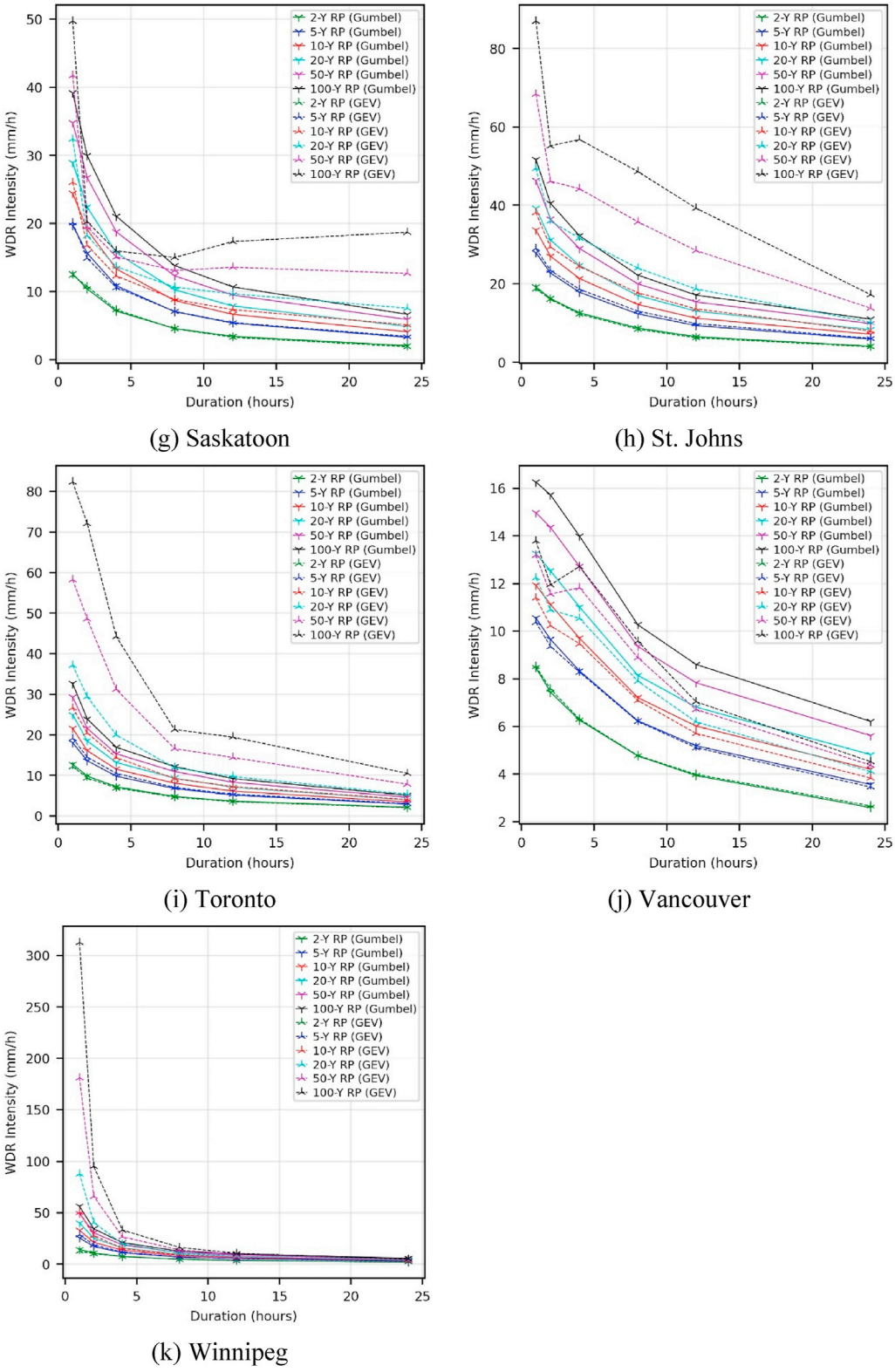

Fig. 5. (*continued*).

compared with the annual maximum hourly wind velocities. In Table 1, the Wind Velocity (%) is the ratio of the annual maximum hourly wind velocity during rain to that of all events averaged over 31 years. In addition, the ratios between the annual maximum wind pressures during rain events and annual maximum wind pressure are denoted as Wind Pressure (%). The wind pressure was calculated using the Bernoulli's principle (Eq. (10)), where P is the calculated wind pressure, ρ is the air density, and v is the wind velocity; the value for air density was assumed to be 1.225 kg/m^3.

$$P = \frac{1}{2}\rho v^2 \tag{10}$$

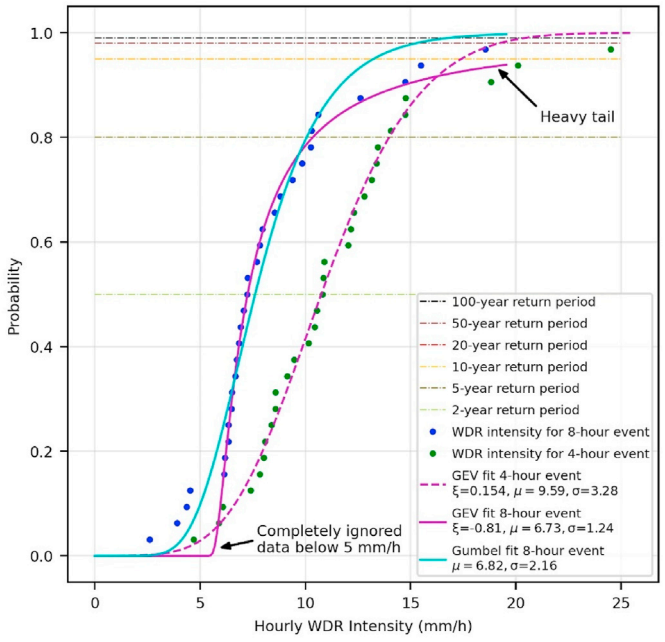

Fig. 6. Fitting plots of WDR intensities for 8-consecutive hourly events in Moncton.

Vancouver had a much higher frequency of rain hours than all other major cities in Canada as were analyzed during the period 1986–2016. Rain events occurred almost 20% of time in this city. Conversely, Calgary had the fewest hours of rain over the same period of time where rain fall only occurred 3.15% of time. The annual maximum hourly wind velocities during rain events were 8.8%–23.9% less than that for all hours. Based on this information, the corresponding hourly wind pressures during rain events were then determined to range between 16.1% and 40.6% from all hours. Halifax had the highest Wind Velocity % and, rain occurred 7.74% over this time period, which was the top 3 amongst these 11 cities. However, Saskatoon received the second least amount of rain for the 31 years whilst having a higher Wind Velocity % than the other 8 cities. From these observations no clear correlation could be concluded between the frequency of rain hours and the ratio of wind velocities for rain events and all hours. The rank of the Wind Pressure % followed the rank of the Wind Velocity % as they were positively correlated through Bernoulli's principle. Theoretically speaking, a higher frequency of rain hours would increase the probability of occurrence of large values for wind velocity during rain events. However, this conjecture was not reflected in this analysis of annual maximum hourly wind velocities.

Hourly DRWPs during rain events and that had a rainfall intensity of more than 0.2 mm/h, defined (by ECCC) as a 'trace' amount of rain which cannot completely wet a surface, were plotted with concurrent rainfall intensities, as shown in Fig. 2. In general, most of the hourly DRWPs during WDR events in all selected cities were less than 100Pa. Over 45% of the hourly DRWPs were less than 10Pa whereas only 3 events had hourly DRWPs that were over 300Pa. Existing watertightness test protocols are required to apply different levels of pressure to test specimens. However, most of these lack consideration for wind pressure acting at relatively low levels. For example, in AAMA 501-05 (2005), the minimum test air pressure is 300Pa. The lowest dynamic pressure step in the European Code EN12865 (EN 12865, 2001) is 0–150Pa and this directly goes to 0–300Pa. Lacasse et al. (2003), used a testing protocol as described in the MEWS project that considered pressure levels under 250Pa, respectively, at 50Pa, 75Pa, and 150Pa. To obtain accurate relationships between real-time WDR conditions and water ingress, more steps at lower pressure levels ought to be considered given that over 50% of wind pressure occurring during rain events are less than 20Pa. The R-squared values for the hourly rainfall intensity and hourly DRWPs were less than 0.1; this indicates that there is no meaningful association that can be established between these two parameters.

3.2. WDR intensity and WDRP index

WDR intensities were calculated by using Eq. (1), assuming that the rain exposure factor, the deposition factor, and the cosine of wind direction equaled 1. The value of the WDRP index was then calculated on the basis of the WDR intensity and concurrent DRWP using Eq. (3), with values of α and β equal to 1. WDR intensities and the corresponding values for hourly WDRP index for each city are shown in Fig. 3.

During the 31 years, only Halifax, Moncton, Toronto, and Winnipeg experienced WDR intensities over 60 mm/h. The maximum WDR intensity of 74 mm/h, was observed in Toronto. Winnipeg reported 3 events with this level of extreme WDR intensity, whereas the other 3 cities, respectively, only experienced WDR of this magnitude once. Frequencies of WDR intensities between 20 mm/h and 60 mm/h in Halifax, St. Johns, and Moncton were, respectively, 95, 58 and 38. However, such levels of WDR intensity only occurred 4 times in Vancouver and 3 times in Montreal although these two cities had the most, and second most, rain hours over the 31 years investigated. In the remaining cities, such frequencies ranged from 11 to 21.

Over 99% of WDR intensities in all cities were less than 20 mm/h, which is equivalent to a water spray rate of 0.7 L/m^2-min for a 10-min period according to that proposed by Linsley et al. (1975) in Eq. (11):

$$\frac{i(t)}{i_h} = \left(\frac{3600}{t}\right)^{\gamma} \tag{11}$$

where $i(t)$ is the rainfall intensity (mm/h) for a particular time interval (s), i_h is the hourly rainfall intensity and the Linsley exponent γ, which is set to 0.42. In these watertightness test standards (ASTM E331-00, 2016; EN 12865, 2001; Lacasse et al., 2003), the minimum specified spray rates were 1.5 L/m^2-min plus 1.2 L/m-min runoff, 1.0 L/m^2-min, and 3.4 L/m^2-min respectively; these were all much larger than the 0.7 L/m^2-min spray rate derived from a WDR intensity of 20 mm/h. In a watertightness test protocol, spray rates at lower levels should be given more consideration when attempting to more accurately correlate the WDR and DRWP to a consequent moisture load. The large hourly values of WDRP index for Calgary, Charlottetown, Halifax, Moncton, Ottawa, and Saskatoon were primarily caused by large values of DRWP during rain events. Moreover, in St. Johns and Winnipeg, the WDR intensity was the major factor that increased the value of the hourly WDRP index. In Montreal, Toronto, and Vancouver, the respective values of hourly WDRP index were lower than other cities. Thus, risks of water ingress for wall assemblies in these locations would also be relatively minor. The trend line in each plot expresses the relative contribution of DRWP and WDR intensity to that of the WDRP index. A steeper trend line, as expressed by slope ratio, implies higher DRWP at the same cumulative probability of occurrence as depicted in Table 2. For instance, St. Johns, Halifax, and Moncton had the highest 3 slope ratios and the DRWPs in these 3 cities were overall, larger than that in other cities, at the same cumulative probability level. Similar conclusions could also be drawn when comparing DRWPs in cities having slope ratios in the 40s to cities having lower values for slope ratio.

3.3. Wind directions during rain events

The averaged wind direction, measured at the same location as the averaged wind speed, is the direction from which the wind blows. The minimum scale of the measured direction is 10°. Prevailing wind directions of each city during rain events are shown in Fig. 4. A wind blowing from the north is denoted as 0-degree, and the 90-degree represents the easterly direction. In Calgary, the prevailing wind direction during rain events was between 0 and 320° and it was found that over 30% of the time the wind was blowing from this range of directions. In

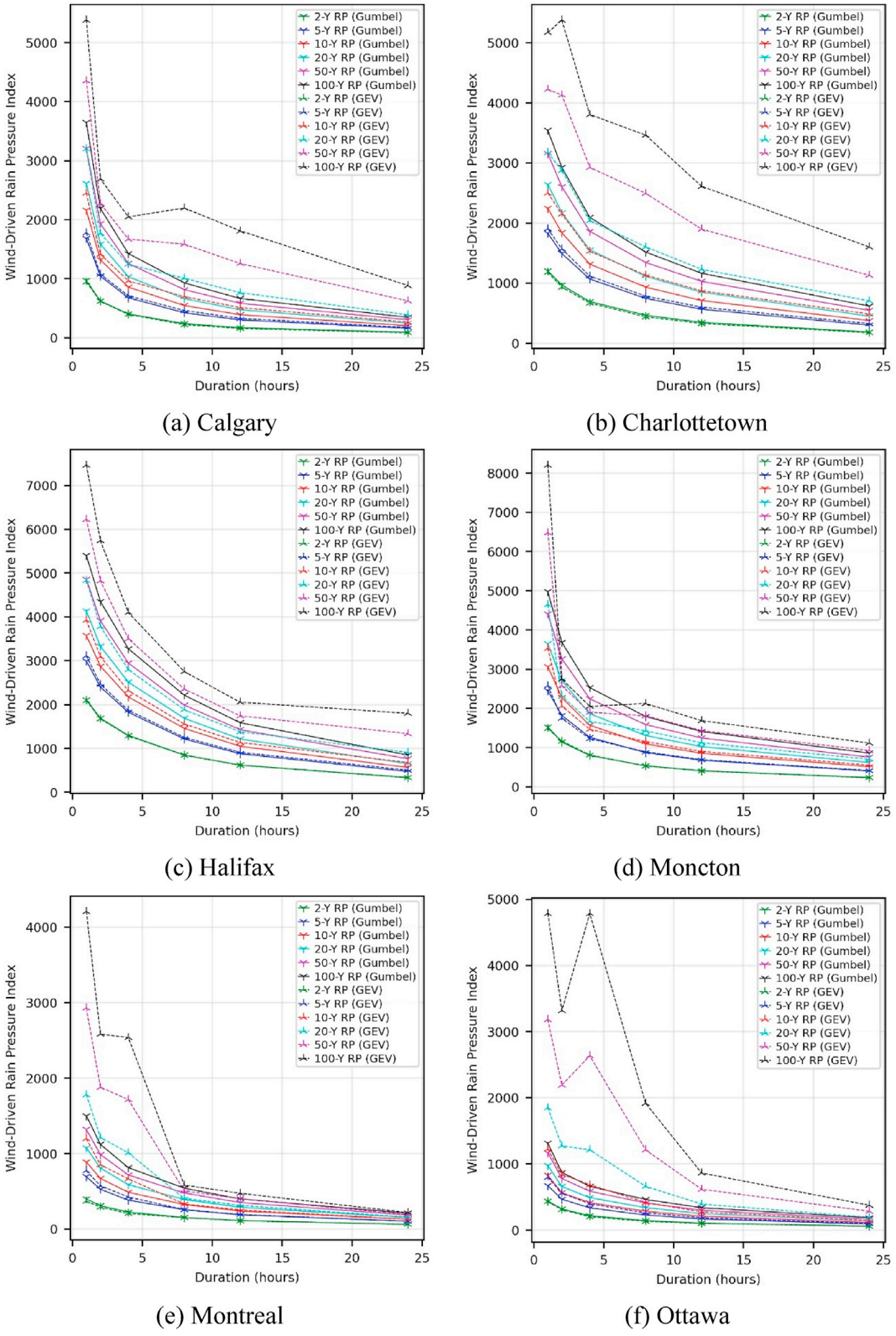

Fig. 7. IDF curves for WDRP index in each city investigated.

Charlottetown, over 40% of the time the wind during rain events were recorded from the south-southeast direction. Most of the wind in Halifax was blowing from the Atlantic Ocean, which is southeast to city. The top 2 prevailing wind directions for Moncton were north and southeast by south. In Montreal, over 50% of the time the wind was blowing from the direction between southeast and southwest, whereas over 10% of that wind was from north-easterly direction. Wind during rain events in Ottawa was recorded mainly from the east-northeast and south by west. In Saskatoon, the north direction alone had over 27% of wind during rain events, whereas 8.5% and 9.5% of the time the wind was blowing,

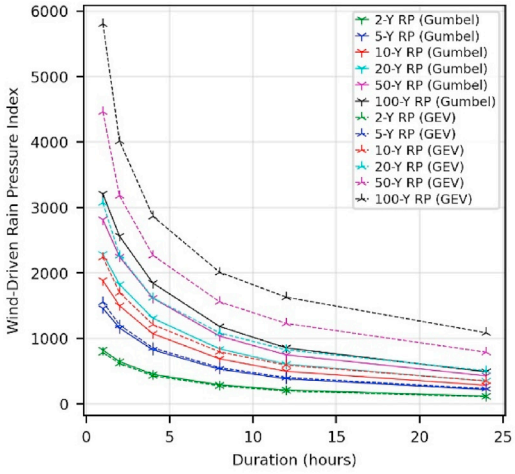

(g) Saskatoon

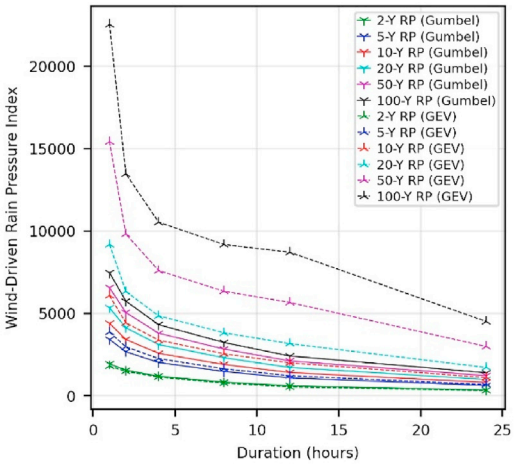

(h) St. Johns

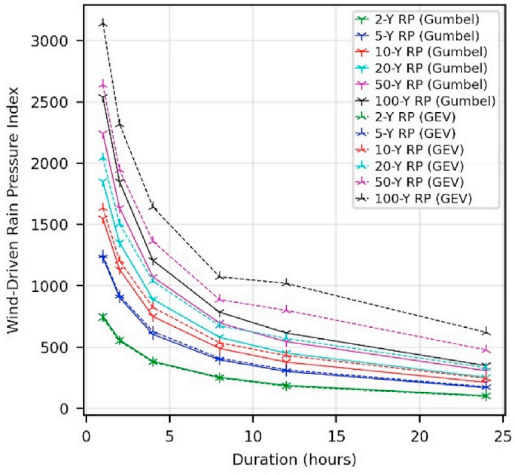

(i) Toronto

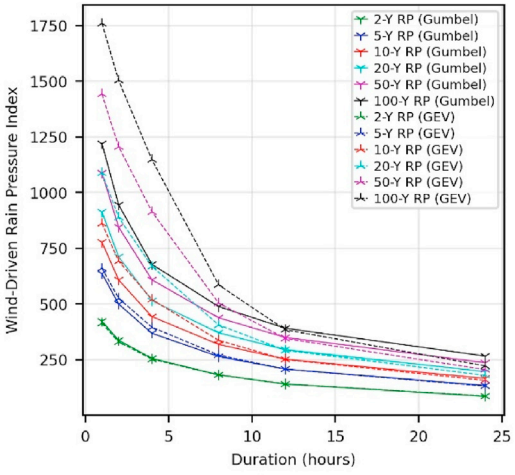

(j) Vancouver

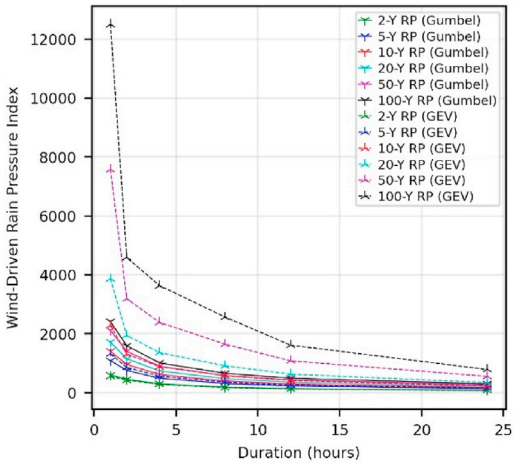

(k) Winnipeg

Fig. 7. (*continued*).

respectively, from the northwest and north-northwest directions. The wind in all other directions occurred less than 5% of the time. The prevailing wind direction during rain events in St. Johns did not blow from the Atlantic Ocean as is the case for Halifax; over 50% of the time the wind was blowing from a direction between southeast and southwest, whereas the ocean is situated directly east of the city. The wind direction in Toronto came from two notable directions: east by north and south-southeast whereas in Vancouver east by north was the only prevailing wind direction. In Winnipeg, wind directions were irregularly distributed over all directions; the wind from the south direction was slightly more frequent than other directions.

Table 4
WDR and WDRP index for 50 and 100-year return period at different durations.

Parameters		WDR		WDRP index	
Cities	Duration	1-hr (mm/h)	24-hr total[a] (mm)	1-hr	24-hr total[a]
Calgary	*50-Year*	44	108	3206	7312
	100-Year	49.6	120	3648	8304
Charlottetown	*50-Year*	30.7	191	3157	13112
	100-Year	33.5	213	3543	14828
Halifax	*50-Year*	38.2	202	3665	17723
	100-Year	41.4	222	4092	19655
Moncton	*50-Year*	36.3	192	4410	18170
	100-Year	39.9	213	4979	20640
Montreal	*50-Year*	23.6	99.8	779	4335
	100-Year	26.4	111	883	4901
Ottawa	*50-Year*	32	93	1169	3963
	100-Year	35.9	102	1313	4466
Saskatoon	*50-Year*	34.8	141	2813	10288
	100-Year	39.2	160	3207	11757
St. Johns	*50-Year*	46.4	237	6558	29304
	100-Year	51.7	264	8471	33447
Toronto	*50-Year*	29.3	110	2243	7394
	100-Year	32.6	121	2537	8364
Vancouver	*50-Year*	15	135	1088	5674
	100-Year	16.3	149	1219	6389
Winnipeg	*50-Year*	49.2	123	2116	6401
	100-Year	56.1	137	2414	7277

[a] Product of 24-h intensity and 24 h.

4. Extreme Value Analysis

A watertightness protocol permits determining the risk (probability of occurrence) and thereafter, the acceptable range of risk of water entry to a wall assembly when subjecting the wall to all possible WDR conditions for a given climate zone or location. Such boundary conditions considering both the magnitude and the probability of occurrence could be derived from the EVA of historical climate data. Semi-empirical and theoretical models have been used to analyze the precipitation and have been validated by hydraulic applications, whereas few efforts have been made to analyze WDR loads and thus no models could be referenced. As such, goodness of fit tests have been added to this analysis to examine the quality of the models being implemented. In addition, an approach is discussed to derive the magnitude of DRWP at a required probability of occurrence, by studying the magnitude and probability of occurrence of concurrent WDR.

The first step of this analysis was to fit the observed datasets with selected distributions for which parameters were obtained through the fitting process. Thereafter, values of events could be calculated by inserting probabilities of occurrence for different return periods into the inverse distribution function using the parameters generated. Annual maximum averaged WDR intensity and hourly WDRP index values for any 1, 2, 4,8,12 and 24 consecutive hours, from the 31-year historical data were used to fit with the Fréchet, Weibull, Gumbel, and Generalized Extreme Value distributions. Their values at 2, 5, 10, 20, 50, and 100-year return periods were then calculated to generate the IDF curves. The averaged WDR intensity for a consecutive hourly event equals the total WDR load collected during these hours divided by the number of hours; the hourly values of WDRP index were also calculated in the same way. The annual maximum values for each type of data were selected from the observed datasets. Thus, for a 31 year period, each dataset would have 31 annual maxima, whereas Cook (1985) has suggested having at least 20 annual maxima when implementing an EVA.

4.1. Goodness of fit tests

The Chi-square test (Pearson, 1900) and Bayesian Information Criterion (BIC) (Schwarz, 1978) were used to exam the goodness of fit for all tested distributions. From the expression of the Chi-square test, a smaller value for χ^2 means a relatively small gap between the observed and expected data generated by a given distribution. Compared to the Chi-square test, the BIC applies a penalty term for the number of parameters in the distribution as it may lead to overfitting of data, for which overfitting is the output of a curve fitting process that comes closely to a portion of the data but may fail thereafter to fit the remainder of the data. Thus, smaller values of BIC represent a greater likelihood of fit.

To select the best distributions to fit the WDR intensity and WDRP index data, the test results for all distributions have been listed together and scores were applied based on their likelihood of occurrence. As shown in Table A.1 and Table A.2 in the Appendix, the distribution with the greatest likelihood for a fitting of one set of data was marked with a green color and given 2 points. The second greatest likelihood for the same set of data was marked with a yellow color and given 1 point. Thus, a greater value for the sum of the scores of a distribution represents the preferred choice to be used to fit the data. A summary of the scores for each distribution type is given in Table 3.

The GEV distribution obtained the highest scores for both goodness of fit test criteria; this means that for most of the cases, the GEV distribution generated a greater likelihood for a good fit than other distributions. In comparison, the Gumbel distribution would be considered the second choice to be used to fit the WDR intensity and WDRPI data, as it received the 2nd highest score amongst these four distributions. It was noted that the Gumbel distribution obtained a higher score under the BIC test than under the Chi-square test, which was attributed to a penalty term applied by the BIC method to the number of parameters in the distributions, given that there are only two parameters in the Gumbel distribution and three parameters in the GEV distribution.

Other than estimating the likelihood of the distributions, the hypothesis test has also been conducted to determine if the sample data are consistent with the hypothesized distributions. The null hypothesis states that the data are consistent with a specified distribution and the alternative hypothesis states that the data are not consistent with a specified distribution. A 0.05 significance level, which is the probability of the test rejecting the null hypothesis, was the criteria for the current test. If the generated value of Chi-square goodness of fit test χ^2_1 is greater than the table value χ^2_2 (Table A.3), the null hypothesis would be rejected. The Chi-square table value was determined based on the significance level and the degree of freedom (DOF). In this study, the DOF for a two-parameter distribution is 28 and for a three-parameter distribution is 27; their corresponding values for χ^2_2 are 41.3 and 40.1 respectively. The maximum Chi-square test value χ^2_1 from Table A.1 is 3.77 which is much

Table 5
Hourly averaged DRWP for 50-year return period.

Cities	Calgary	Charlottetown	Halifax	Moncton	Montreal	Ottawa
DRWP (Pa)	189	196	235	225	124	94.5
Cities	Saskatoon	St. Johns	Toronto	Vancouver	Winnipeg	
DRWP (Pa)	201	324	156	118	159	

lower than values given in Table A.3. As such, the null hypothesis was accepted. No significant difference could be found between the observed data and the data generated from the distribution.

4.2. IDF and extreme values

The Gumbel and GEV distributions, which obtained higher scores than the other two distributions, have been used to generate IDF curves to provided information of WDR intensities and WDRPI for each consecutive hourly event. WDR intensities for 1-h and 24-consecutive hourly events, respectively representing the upper and lower limits of rain events, varied markedly in different cities, as shown in Fig. 5. For 1-h events, and for all return periods, the cities of St. Johns and Winnipeg, both distributions generated higher WDR intensities than any of the other cities. Between these two cities, WDR intensities for 2-year, 5-year and 10-year return periods in St. Johns were greater than those obtained for Winnipeg and conversely smaller for 20-year, 50-year and 100-year return periods. The maximum WDR intensities observed in Winnipeg for the 100-year return period were 56.1 mm/h from the Gumbel distribution and 312.6 mm/h from the GEV distribution; the significant difference between the values obtained from the respective distributions is discussed in more detail in the subsequent section. Additionally, for WDR intensities during 24-consecutive hourly events, the largest values were observed in St. Johns; 11 mm/h from the Gumbel distribution and 17.3 mm/h from the GEV distribution. The WDR load within 24 h in St. Johns was 264 mm and 451.2 mm derived from the Gumbel and GEV distributions, respectively. A larger value of 18.7 mm/h from the GEV distribution was also noted for Saskatoon. However, such a value was generated by a poor fitting which will next be discussed.

In all the above extreme WDR values, the GEV distribution generated a much more conservative value than that of the Gumbel distribution in Calgary, Montreal, Saskatoon, St. Johns, Toronto, and Winnipeg. Some 'spikes' in the curves generated by the GEV distribution were also noted in: Halifax, Moncton, Montreal, and Vancouver for 50-year and 100-year return periods where WDR intensities at a given duration were larger than that for an adjacent and smaller duration; this is not possible from the observational data, as the averaged value from a longer duration event is always smaller than the average value from a shorter duration event. The reason for such phenomena was mainly attributed to the lack of limitation of the heaviness of distribution tails estimated through the shape factor in the GEV distribution equation. For example, the WDR intensities generated by the GEV distribution in Moncton for the 8-consecutive hourly events at 20-year, 50-year and 100-year return periods were larger than the WDR intensities generated by the same distribution for 4-consecutive hourly events, as well as larger than the WDR intensities generated by the Gumbel distribution for 8-consecutive hourly events, as shown in Fig. 5 (d).

Fitting plots of the three, previously mentioned, cases are presented in Fig. 6. The probabilities of occurrence for each return period, are also marked in the plot. It is evident that the tail of the GEV distribution for 8-consecutive hourly events is "heavier" than that of the Gumbel distribution for the same event, as well as, the tail of the GEV distribution for 4-consecutive hourly events. Consequently, the value for WDR intensity generated by the GEV distribution, as fitted to the 8-hourly events were much higher than that generated by the GEV distribution fitted to the 4-hourly events and as well, the Gumbel distribution fitted to the 8-hourly events at a 100-year return period (probability of occurrence 0.99). The shape factor ζ of the Gumbel distribution has a constant value of 0, which resulted in changing the tail of the Gumbel distribution to be monotonic; this is a prerequisite for the monotonicity of WDR intensities in the IDF curves. Overfitting is another issue observed in the GEV distribution plots. The GEV distribution fitted values extremely well for hourly WDR intensity larger than 5 mm/h, whereas it completely failed to fit values for WDR intensity of less than 5 mm/h. For the same case, the Gumbel distribution balanced the fitting for each portion of the data thereby providing a smoother and indeed, monotonical change of WDR intensities in the IDF curves. Given these observations, the Gumbel distribution was considered a better choice than the GEV distribution to fit with WDR data to be used for generating the IDF curves.

In Fig. 7, the IDF curves are shown for the hourly WDRP index for the different cities; fittings of values for hourly WDRP index as a function of rain duration (h) are plotted for both the GEV and Gumbel distributions. In most of the scenarios, the GEV distribution generated greater hourly values of WDRP index, as compared to that generated using the Gumbel distribution; this could be determined from controlling tails of the distributions and overfitting, as previously discussed. The highest value for hourly WDRP index occurred in St. Johns for all return periods, all hourly duration events, and for both distributions. The values for WDRP indices with a 100-year return period generated by the GEV and Gumbel distributions respectively were, for 1-h events 22529 and 7470, respectively, and for 24-consecutive hourly events these were 4510 and 1393, respectively.

Overall, the Gumbel distribution is considered a better option for EVA, as it had a higher score than the Fréchet and Weibull distributions from the goodness of fit test. Also, Gumbel distribution supresses overfitting during the fitting process; this is an essential element to permit generating monotonic and smooth curves to be used for IDF plots.

Extreme values generated by the Gumbel distribution in each city obtained from the analysis are depicted in Table 4. For the 50-year and 100-year return periods, the highest WDR intensities for 1-h events were, respectively, 49.2 mm/h and 56.1 mm/h, both of which occurred in Winnipeg. Whereas St. Johns had the greatest WDR load of 237 mm and 264 mm, respectively, for the 50-year and 100-year return periods, within 24 h and the second highest WDR intensities. Additionally, the most extreme WDR conditions, represented by the WDRP index, were also observed in St. Johns. Overall, St. Johns had a greater chance to experience more severe WDR conditions than most cities in Canada that were studied using the EVA. The extreme WDR intensity obtained for Vancouver was much lower than any other cities whereas the total WDR load over 24 h ranked 5th amongst the 11 cities studied, this being attributed to the higher frequency of rain events in this location. Wall assemblies in Montreal were exposed to the least severe WDR conditions over the studied period of 31 years, given that the value of the hourly WDRP index was the smallest of all cities examined, whereas Ottawa had the least cumulative value for WDRP index over 24-h rain events.

4.3. Extreme DRWP

As discussed in the previous sections, no meaningful correlations could be established between the rainfall intensity and DRWP. In other words, the magnitude and the occurrence of DRWP were independent of the magnitude and occurrence of WDR intensity. Thus, the output of the EVA for the DRWP could not be associated with the output of the EVA for the WDR intensity. The moisture load to which wall assemblies are subjected is the result of the simultaneous action of both WDR and DRWP. The 'co-occurrence' of these actions ought to be taken into account when deriving the magnitude of these two parameters. The WDRP index represents the joint action of WDR concurrent with the DRWP and were used to balance the relative magnitudes of these two parameters. The maximum value of the WDRP index permits determining the extent of influence of the two concurrent climate load parameters in respect to the risk of water entry, and such a limit was not necessarily the upper limit for the uncorrelated parameters. For instance, the maximum value for the WDRP index in St. Johns was 10096, as shown in Fig. 3(h). The WDR intensity and concurrent DRWP for this event were 44.8 mm/h and 225Pa respectively, whereas, as shown in Table 2, the maximum value of WDR intensity and maximum value of DRWP were 54.4 mm/h and 288Pa respectively. The events with the maximum WDR intensity and the maximum DRWP may not render the worst WDR conditions, which is reflected by the value of the WDRP index. Thus, a reasonable DRWP magnitude should be derived from the relevant values of WDR intensity and the WDRP index.

As given in Eq. (5), the DRWP could be calculated from the WDRP index, by knowing the magnitude of the WDR intensity. However, once the EVA is applied, the probabilities of occurrence of these 3 parameters also need to be considered. A 100-year return period represents a 1% probability of occurrence of an event within a year. If the event was derived from two uncorrelated events, then the product of probabilities of occurrence of the two events also has to be 1%. Thus, to obtain the DRWP for a 50-year return period (2% probability of occurrence), the corresponding WDR intensity and the WDRP index used in the calculation should be for a 2-year return period (50% probability of occurrence) and 100-year return period respectively (1% probability of occurrence). The DRWP calculated based on the values of WDRP index at a 100-year return period and 2-year return period of WDR, as listed in Table 5. The highest hourly DRWP during 1-h events for a 50-year return period was observed in St. Johns, the value of which was 324 Pa. The second highest DRWP was obtained in another coastal city, Halifax, whereas Ottawa had the smallest value of DRWP amongst the 11 cities evaluated in this paper.

5. Conclusions

Detailed WDR conditions, as occurred between 1986 and 2016, for 11 major cities located in Canada were described and discussed in this paper. The magnitude of rainfall intensity, DRWP, and WDR intensity, as well as the corresponding frequencies and probabilities of occurrence of rain events, varied considerably amongst the different cities, given their differences in geographic location and hence differences in regional climate.

Vancouver had more rain hours than all the other cities, while having the smallest WDR intensity at the same probability of occurrence. The wind velocity determined during rain events was established not to be relevant in respect to the frequency of rain events, although, in general, the cities with more rain hours should have a higher probability to encounter greater wind velocities. The histograms of rainfall intensity and wind velocity during rain events revealed that the most frequent wind velocity during rain events was less than 5 m/s in all cities, whereas no meaningful correlation could be established between these two parameters. Over 90% of rain events in all cities had a WDR intensity of less than 5 mm/h. The distribution of values for WDRP index indicated that St. Johns had a higher probability to experience more severe WDR conditions than all the other locations studied. The magnitude of parameters obtained from the analysis suggest that greater consideration should be given to more temperate WDR conditions when undertaking a watertightness test.

The Fréchet, Weibull, Gumbel and GEV distributions were used to fit the historical WDR and WDRP index data for the cities, as analyzed in this study. The performance of each distribution was assessed by the goodness of fit test using the Chi-square test and Bayesian information criterion. The Gumbel and GEV distributions were both selected to be used in the EVA to generate the IDF curves for the WDR and WDRP index, as these distributions provided a better fit to the relationships than the Fréchet and Weibull distributions. Although, the hypothesis test suggested no significant difference could be found between the observed data and the data generated by all four distributions. After comparing the data generated by the Gumbel and GEV distributions, it was found that for the GEV distribution overfittings and regularly occurring “heavy tails” were evident from the fitting process. This led to obtaining non-monotonic curves for the IDF plots. Thus, only values generated by the Gumbel distribution were subsequently used for the analysis. As such, St. Johns had a greater probability to experience larger values for hourly WDRP index, DRWP, WDR load and 24-h WDRP index, than all other cities examined in this study, whereas the most severe WDR intensities for 50-year and 100-year return periods were observed for Winnipeg.

Boundary conditions of WDR related parameters obtained in these studies will contribute to the development a watertightness test protocol that will permit establishing relationships between the climate loads acting on buildings and moisture loads in wall assemblies.

CRediT authorship contribution statement

Zhe Xiao: Conceptualization, Methodology, Software, Formal analysis, Investigation, Data curation, Writing – original draft, preparation, Visualization. **Michael A. Lacasse:** Supervision, Writing – review & editing. **Elena Dragomirescu:** Supervision, Writing – review & editing.

Declaration of competing interest

The authors declare that they have no known competing financial interests or personal relationships that could have appeared to influence the work reported in this paper.

Acknowledgements

I would like to thank Dr. Abhishek Gaur, for his assistance in acquiring the meteorological data and advice in doing the subsequent data analysis. My grateful thanks are also extended to Mr. Reid Paxton for his help in establishing the code to quickly generate results from such a large amount of data.

This work is a part of the Climate-Resilient Buildings and Core Public Infrastructure (CRBCPI) project supported by the National Research Council Canada’s Construction Research Centre (CRC) and Infrastructure Canada.

Appendix B. Supplementary data

Supplementary data to this article can be found online at https://doi.org/10.1016/j.jweia.2021.104611.

Appendix A

Table A.1
Chi-Square test results

Chi-Square Test		WDR						WDRP					
Cities	Durations	1H	2H	4H	8H	12H	24H	1H	2H	4H	8H	12H	24H
CAL	**Fréchet**	0.077	0.075	0.267	0.503	0.133	0.742	0.112	0.179	1.753	0.317	0.141	0.112
	Weibull	0.194	0.286	0.152	0.159	0.137	0.265	0.107	0.134	0.133	0.250	0.248	0.218
	GBL	0.126	0.104	0.086	0.087	0.102	0.171	0.146	0.165	0.150	0.236	0.244	0.253
	GEV	0.051	0.067	0.081	0.087	0.102	0.163	0.106	0.141	0.109	0.056	0.022	0.034

(*continued on next column*)

Table A.1 (*continued*)

Chi-Square Test		WDR						WDRP					
Cities	Durations	1H	2H	4H	8H	12H	24H	1H	2H	4H	8H	12H	24H
CHAR	**Fréchet**	0.282	0.389	0.112	0.428	0.137	0.876	0.760	0.081	0.291	0.168	0.069	0.063
	Weibull	0.083	0.071	0.187	0.239	0.241	0.523	0.197	0.197	0.373	0.364	0.311	0.326
	GBL	0.107	0.113	0.109	0.163	0.166	0.217	0.094	0.146	0.231	0.238	0.208	0.161
	GEV	0.073	0.070	0.097	0.147	0.125	0.172	0.046	0.076	0.173	0.130	0.061	0.052
HALI	**Fréchet**	0.246	0.211	0.868	0.327	0.854	0.366	0.582	0.716	1.331	1.835	0.249	0.313
	Weibull	0.101	0.382	0.259	0.218	0.134	0.115	0.287	0.186	0.180	0.129	0.155	0.217
	GBL	0.049	0.044	0.107	0.090	0.066	0.025	0.156	0.134	0.158	0.148	0.210	0.224
	GEV	0.042	0.036	0.107	0.089	0.064	0.023	0.156	0.132	0.149	0.125	0.139	0.201
MONC	**Fréchet**	0.252	0.241	0.112	0.328	0.238	0.391	0.407	0.115	0.590	0.613	0.090	3.605
	Weibull	0.146	0.202	0.083	0.292	0.112	0.053	0.142	0.100	0.092	0.075	0.056	0.066
	GBL	0.066	0.173	0.076	0.316	0.186	0.079	0.097	0.107	0.102	0.088	0.079	0.097
	GEV	0.066	0.152	0.060	0.327	0.103	0.049	0.059	0.104	0.099	0.069	0.049	0.058
MONT	**Fréchet**	1.041	0.563	0.109	0.082	0.168	0.180	0.405	0.398	0.187	0.433	0.415	0.323
	Weibull	0.907	0.783	0.826	0.302	0.263	0.524	0.379	0.292	0.299	0.405	0.472	0.263
	GBL	0.467	0.562	0.328	0.082	0.185	0.243	0.428	0.270	0.397	0.396	0.458	0.254
	GEV	0.213	0.172	0.107	0.053	0.140	0.148	0.128	0.112	0.089	0.259	0.337	0.214
OTT	**Fréchet**	0.074	0.485	1.778	1.506	3.768	0.060	0.244	0.206	0.128	0.138	0.088	0.287
	Weibull	0.075	0.256	0.576	0.316	0.082	0.290	0.373	0.204	0.554	0.401	0.305	0.205
	GBL	0.055	0.072	0.229	0.123	0.052	0.090	0.203	0.171	0.304	0.302	0.195	0.197
	GEV	0.055	0.051	0.102	0.092	0.050	0.060	0.155	0.164	0.112	0.129	0.060	0.099
SASK	**Fréchet**	1.084	0.370	0.115	0.423	0.388	0.174	0.741	1.236	1.753	0.860	0.578	0.388
	Weibull	0.168	0.103	0.083	0.113	0.285	0.447	0.087	0.080	0.135	0.095	0.110	0.143
	GBL	0.095	0.151	0.076	0.087	0.216	0.321	0.222	0.228	0.243	0.206	0.197	0.320
	GEV	0.064	0.108	0.068	0.086	0.203	0.153	0.061	0.068	0.100	0.084	0.067	0.046
ST.J	**Fréchet**	0.108	0.247	0.093	0.086	0.072	0.370	0.186	0.046	0.207	0.187	0.206	0.380
	Weibull	0.370	0.307	0.388	0.580	0.939	0.421	0.334	0.129	0.288	0.291	0.527	0.669
	GBL	0.173	0.116	0.161	0.261	0.261	0.218	0.282	0.208	0.187	0.354	0.425	0.616
	GEV	0.062	0.109	0.083	0.085	0.069	0.096	0.062	0.045	0.094	0.055	0.076	0.115
TOR	**Fréchet**	0.077	0.184	0.082	0.112	0.104	0.109	0.081	0.563	1.553	1.059	0.077	0.267
	Weibull	0.740	1.190	0.904	0.439	0.519	0.531	0.104	0.146	0.109	0.082	0.109	0.229
	GBL	0.276	0.615	0.285	0.187	0.150	0.235	0.126	0.133	0.080	0.059	0.096	0.174
	GEV	0.073	0.134	0.074	0.103	0.091	0.095	0.078	0.126	0.063	0.058	0.064	0.072
VAN	**Fréchet**	0.295	0.179	1.066	0.174	0.177	0.261	0.164	0.421	0.208	0.245	0.145	0.115
	Weibull	0.098	0.272	0.356	0.105	0.069	0.080	0.374	0.315	0.215	0.241	0.128	0.121
	GBL	0.154	0.169	0.140	0.118	0.159	0.165	0.216	0.168	0.119	0.227	0.128	0.114
	GEV	0.075	0.169	0.118	0.072	0.066	0.079	0.107	0.093	0.102	0.226	0.122	0.106
WINNI	**Fréchet**	0.241	0.133	0.168	0.518	1.712	0.802	0.113	0.073	0.061	0.067	0.075	0.107
	Weibull	0.464	0.220	0.277	0.140	0.169	0.071	0.210	0.146	0.215	0.489	0.267	0.243
	GBL	0.571	0.137	0.148	0.060	0.127	0.078	0.358	0.145	0.199	0.318	0.287	0.254
	GEV	0.181	0.085	0.142	0.058	0.126	0.067	0.079	0.038	0.051	0.065	0.061	0.051

Table A.2
BIC test results

BIC		WDR						WDRP					
Cities	Durations	1H	2H	4H	8H	12H	24H	1H	2H	4H	8H	12H	24H
CAL	**Fréchet**	−175	−176	−137	−117	−159	−105	−164	−149	−79	−132	−157	−164
	Weibull	−147	−135	−155	−153	−158	−137	−165	−158	−159	−139	−139	−143
	GBL	−164	−170	−175	−175	−170	−154	−159	−155	−158	−144	−143	−142
	GEV	−188	−180	−174	−172	−167	−152	−166	−157	−165	−186	−214	−201
CHAR	**Fréchet**	−135	−125	−164	−122	−158	−100	−105	−174	−134	−151	−179	−182
	Weibull	−173	−178	−148	−141	−140	−116	−147	−147	−127	−127	−132	−131
	GBL	−169	−167	−168	−156	−155	−147	−173	−159	−145	−144	−148	−156
	GEV	−177	−179	−169	−156	−161	−151	−192	−176	−151	−159	−183	−188
HALI	**Fréchet**	−140	−144	−101	−131	−101	−127	−113	−106	−87	−77	−139	−132
	Weibull	−167	−126	−138	−143	−158	−163	−135	−148	−149	−160	−154	−144
	GBL	−193	−197	−169	−174	−184	−214	−157	−162	−157	−159	−148	−146
	GEV	−194	−199	−165	−171	−182	−213	−154	−159	−155	−161	−157	−146

(*continued on next column*)

Table A.2 (*continued*)

BIC		WDR						WDRP					
Cities	Durations	1H	2H	4H	8H	12H	24H	1H	2H	4H	8H	12H	24H
MONC	**Fréchet**	−139	−140	−164	−131	−141	−125	−124	−163	−113	−111	−171	−56
	Weibull	−156	−146	−173	−134	−164	−187	−157	−168	−170	−176	−185	−180
	GBL	−184	−154	−179	−135	−152	−178	−172	−169	−170	−175	−178	−172
	GEV	−181	−155	−183	−131	−167	−190	−184	−166	−168	−179	−190	−184
MONT	**Fréchet**	−95	−114	−165	−174	−151	−149	−124	−125	−148	−122	−123	−131
	Weibull	−99	−104	−102	−133	−138	−116	−126	−134	−134	−124	−119	−137
	GBL	−123	−117	−134	−177	−152	−143	−126	−140	−128	−128	−124	−142
	GEV	−144	−151	−165	−187	−157	−155	−160	−164	−171	−138	−130	−144
OTT	**Fréchet**	−177	−119	−78	−83	−55	−183	−140	−145	−160	−158	−172	−135
	Weibull	−176	−138	−113	−132	−174	−134	−127	−145	−114	−125	−133	−145
	GBL	−190	−181	−145	−165	−191	−174	−149	−154	−136	−137	−150	−150
	GEV	−186	−188	−167	−170	−189	−183	−154	−152	−164	−160	−184	−168
SASK	**Fréchet**	−94	−127	−163	−123	−126	−150	−105	−90	−79	−101	−113	−125
	Weibull	−151	−167	−173	−164	−135	−121	−172	−174	−158	−169	−165	−156
	GBL	−172	−158	−180	−175	−147	−135	−146	−145	−143	−149	−150	−135
	GEV	−181	−165	−179	−172	−146	−154	−183	−179	−167	−173	−180	−192
ST.J	**Fréchet**	−165	−140	−170	−172	−178	−127	−148	−191	−145	−148	−145	−126
	Weibull	−127	−133	−126	−113	−98	−123	−130	−160	−135	−134	−116	−109
	GBL	−154	−166	−156	−141	−141	−147	−139	−148	−152	−132	−126	−115
	GEV	−182	−165	−173	−173	−179	−169	−182	−193	−170	−186	−176	−163
TOR	**Fréchet**	−176	−149	−174	−164	−166	−165	−174	−114	−83	−94	−176	−137
	Weibull	−105	−91	−99	−122	−116	−116	−166	−156	−165	−174	−165	−142
	GBL	−140	−115	−138	−152	−158	−144	−164	−162	−178	−187	−172	−154
	GEV	−177	−158	−177	−167	−170	−169	−175	−160	−182	−185	−181	−178
VAN	**Fréchet**	−134	−149	−94	−150	−150	−138	−152	−123	−145	−140	−156	−163
	Weibull	−168	−136	−128	−166	−179	−175	−127	−132	−144	−140	−160	−162
	GBL	−158	−155	−160	−166	−157	−155	−147	−155	−166	−146	−163	−167
	GEV	−176	−151	−162	−178	−181	−175	−165	−170	−167	−142	−161	−166
WINNI	**Fréchet**	−140	−159	−151	−117	−79	−103	−164	−177	−183	−180	−177	−165
	Weibull	−120	−143	−136	−157	−151	−178	−145	−156	−144	−118	−137	−140
	GBL	−117	−161	−159	−187	−164	−179	−131	−159	−150	−135	−138	−142
	GEV	−149	−172	−157	−184	−160	−180	−175	−197	−189	−181	−183	−189

Table A.3
Critical values of the Chi-square distribution with df degree of freedom

Level of Significance α								
Df	0.200	0.100	0.075	0.050	0.025	0.010	0.005	0.001	0.0005
1	1.642	2.706	3.170	3.841	5.024	6.635	7.879	10.828	12.116
2	3.219	4.605	5.181	5.991	7.378	9.210	10.597	13.816	15.202
3	4.642	6.251	6.905	7.815	9.348	11.345	12.838	16.266	17.731
4	5.989	7.779	8.496	9.488	11.143	13.277	14.860	18.467	19.998
5	7.289	9.236	10.008	11.070	12.833	15.086	16.750	20.516	22.106
6	8.558	10.645	11.466	12.592	14.449	16.812	18.548	22.458	24.104
7	9.803	12.017	12.883	14.067	16.013	18.475	20.278	24.322	26.019
8	11.030	13.362	14.270	15.507	17.535	20.090	21.955	26.125	27.869
9	12.242	14.684	15.631	16.919	19.023	21.666	23.589	27.878	29.667
10	13.442	15.987	16.971	18.307	20.483	23.209	25.188	29.589	31.421
11	14.631	17.275	18.294	19.675	21.920	24.725	26.757	31.265	33.138
12	15.812	18.549	19.602	21.026	23.337	26.217	28.300	32.910	34.822
13	16.985	19.812	20.897	22.362	24.736	27.688	29.820	34.529	36.479
14	18.151	21.064	22.180	23.685	26.119	29.141	31.319	36.124	38.111
15	19.311	22.307	23.452	24.996	27.488	30.578	32.801	37.698	39.720
16	20.465	23.542	24.716	26.296	28.845	32.000	34.267	39.253	41.309
17	21.615	24.769	25.970	27.587	30.191	33.409	35.719	40.791	42.881
18	22.760	25.989	27.218	28.869	31.526	34.805	37.157	42.314	44.435
19	23.900	27.204	28.458	30.144	32.852	36.191	38.582	43.821	45.974
20	25.038	28.412	29.692	31.410	34.170	37.566	39.997	45.315	47.501
21	26.171	29.615	30.920	32.671	35.479	38.932	41.401	46.798	49.013
22	27.301	30.813	32.142	33.924	36.781	40.289	42.796	48.269	50.512
23	28.429	32.007	33.360	35.172	38.076	41.639	44.182	49.729	52.002
24	29.553	33.196	34.572	36.415	39.364	42.980	45.559	51.180	53.480
25	30.675	34.382	35.780	37.653	40.646	44.314	46.928	52.620	54.950
26	31.795	35.563	36.984	38.885	41.923	45.642	48.290	54.053	56.409

(*continued on next column*)

Table A.3 (*continued*)

Level of Significance α									
27	32.912	36.741	38.184	40.113	43.195	46.963	49.645	55.477	57.860
28	34.027	37.916	39.380	41.337	44.461	48.278	50.994	56.894	59.302
29	35.139	39.087	40.573	42.557	45.722	49.588	52.336	58.302	60.738
30	36.250	40.256	41.762	43.773	46.979	50.892	53.672	59.704	62.164
40	47.269	51.805	53.501	55.759	59.342	63.691	66.766	73.403	76.097
50	58.164	63.167	65.030	67.505	71.420	76.154	79.490	86.662	89.564
60	68.972	74.397	76.411	79.082	83.298	88.380	91.952	99.609	102.698
70	79.715	85.527	87.680	90.531	95.023	100.425	104.215	112.319	115.582
80	90.405	96.578	98.861	101.880	106.629	112.329	116.321	124.842	128.267
90	101.054	107.565	109.969	113.145	118.136	124.117	128.300	137.211	140.789
100	111.667	118.498	121.017	124.342	129.561	135.807	140.170	149.452	153.174

References

AAMA 501-05, 2005. Methods of Tests for Exterior Walls. American Architectural Manufacturers Association, Schaumburg, IL.

Abuku, M., Blocken, B., Poesen, J., Roels, S., 2009a. Spreading, splashing and bouncing of wind-driven raindrops on building facades. In: 11th Am. Conf. Wind Eng..

Abuku, M., Janssen, H., Roels, S., 2009b. Impact of wind-driven rain on historic brick wall buildings in a moderately cold and humid climate: numerical analyses of mould growth risk, indoor climate and energy consumption. Energy Build. 41, 101–110. https://doi.org/10.1016/j.enbuild.2008.07.011.

ASHRAE, 2016. ASHRAE standard 160P-criteria for moisture control design analysis in buildings. ASHRAE Trans.

ASTM E331-00, 2016. Standard Test Method for Structural Performance of Exterior Windows , Curtain Walls , and Doors by Uniform Static Air Pressure Difference. ASTM International, West Conshohocken, PA. https://doi.org/10.1520/E0331-00R16.

Blocken, B., Carmeliet, J., 2006. The influence of the wind-blocking effect by a building on its wind-driven rain exposure. J. Wind Eng. Ind. Aerod. 94, 101–127. https://doi.org/10.1016/j.jweia.2005.11.001.

Blocken, B., Carmeliet, J., 2005. High-resolution wind-driven rain measurements on a low-rise building—experimental data for model development and model validation. J. Wind Eng. Ind. Aerod. 93, 905–928. https://doi.org/10.1016/j.jweia.2005.09.004.

Blocken, B., Carmeliet, J., 2004. A review of wind-driven rain research in building science. J. Wind Eng. Ind. Aerod. 92, 1079–1130. https://doi.org/10.1016/j.jweia.2004.06.003.

Blocken, B., Dezsö, G., van Beeck, J., Carmeliet, J., 2009. The mutual influence of two buildings on their wind-driven rain exposure and comments on the obstruction factor. J. Wind Eng. Ind. Aerod. 97, 180–196. https://doi.org/10.1016/j.jweia.2009.06.003.

Boardman, C.R., Glass, S.V., 2013. Investigating wind-driven rain intrusion in walls with the CARWASh. Therm. Perform. Exter. Envel. Whole Build. - 12th Int. Conf.

Bossche, N. Van Den, Lacasse, M., Moore, T., Janssens, A., 2012. Water infiltration through openings in a vertical plane under static boundary conditions. In: Proceedings of the 5th IBPC. Kyoto, Japan.

Charola, A.E., Lazzarini, L., 1986. Deterioration of brick masonry caused by acid rain. In: ACS Symposium Series, pp. 250–258. https://doi.org/10.1021/bk-1986-0318.ch017.

Choi, E.C.C., 1994. Characteristics of the co-occurrence of wind and rain and the driving-rain index. J. Wind Eng. Ind. Aerod. 53, 49–62. https://doi.org/10.1016/0167-6105(94)90018-3.

Chouinard, K.L., Lawton, M.D., 2001. Rotting wood framed apartments-Not just a Vancouver problem. Proc 8th Can. Conf. Build. Sci. Technol. 304–318.

Chow, V. Te, 1962. Hydrologic determination of waterway areas for the design of drainage structures in small drainage basins. Eng. Exp. Stn. Bull. 462, 104.

Cook, N.J., 1985. The Designer's Guide to Wind Loading of Building Structures. Part 1: Background, Damage Survey, Wind Data and Structural Classification.

Cornick, S.M., Lacasse, M.A., 2010. An investigation of climate loads on building Façades for selected locations in the United States, 19428-2959. In: Symposium on "Up against the Wall": an Examination of Building Envelope Interface. ASTM International, 100 Barr Harbor Drive. PO Box C700, West Conshohocken, PA, pp. 12–36. https://doi.org/10.1520/STP48941S, 12.

Desjarlais, A.O., Karagiozis, A.N., Aoki-Kramer, M., 2001. Wall Moisture Problems in Seattle. Build. VIII Proceedings. ASHRAE, p. 8.

EN 12865, 2001. BS EN 12865:2001 Hygrothermal performance of building components and building elements. Determination of the resistance of external wall systems to driving rain under pulsating air pressure. Building Research Establishment.

Franke, L., Schumann, I., Hees, R. van, Klugt, L. van der, Naldini, S., Binda, L., Balen, K. van, Baronio, G., Mateus, J., 1998. Damage Atlas: Classification and Analyses of Damage Patterns Found in Brick Masonry, Protection and Conservation of European Cultural Heritage, ume 2. Fraunhofer IRB Verlag. Research Report No. 8.

Ge, H., Chiu, V., Stathopoulos, T., Souri, F., 2018. Improved assessment of wind-driven rain on building façade based on ISO standard with high-resolution on-site weather data. J. Wind Eng. Ind. Aerod. 176, 183–196. https://doi.org/10.1016/j.jweia.2018.03.013.

Ge, H., Deb Nath, U.K., Chiu, V., 2017. Field measurements of wind-driven rain on mid- and high-rise buildings in three Canadian regions. Build. Environ. 116, 228–245. https://doi.org/10.1016/j.buildenv.2017.02.016.

Hoppestad, S., 1955. Slagregn I Norge. Norwegian Building Research Institute, Oslo.

ISO, 2009. ISO 15927-3, Hygrothermal Performance of Buildings Calculation and Presentation of Climatic Data Part 3: Calculation of a Driving Rain Index for Vertical Surfaces from Hourly Wind and Rain Data.

Karagiozis, A., Hadjisophocleous, G., Cao, S., 1997. Wind-driven rain distributions on two buildings. J. Wind Eng. Ind. Aerod. 67–68, 559–572. https://doi.org/10.1016/S0167-6105(97)00100-1.

Kubilay, A., Derome, D., Blocken, B., Carmeliet, J., 2015. Wind-driven rain on two parallel wide buildings: field measurements and CFD simulations. J. Wind Eng. Ind. Aerod. 146, 11–28. https://doi.org/10.1016/j.jweia.2015.07.006.

Kubilay, A., Derome, D., Blocken, B., Carmeliet, J., 2014. High-resolution field measurements of wind-driven rain on an array of low-rise cubic buildings. Build. Environ. 78, 1–13. https://doi.org/10.1016/j.buildenv.2014.04.004.

Lacasse, M.A., O'Connor, T., Nunes, S.C., Beaulieu, P., 2003. Report from task 6 of MEWS project: experimental assessment of water penetration and entry into wood-frame wall specimens - final report. Research Report (National Research Council of Canada. Institute for Research in Construction); no. RR-133.

Lacy, R.E., 1977. Climate and Building in Britain. In: Her Majesty's Stationery Office. John Wiley & Sons, Ltd, London. https://doi.org/10.1002/qj.49710544325.

Linsley, R., Kohler, M., JLH, P., 1975. Applied Hydrology. McGraw-Hill, New York, US.

Mayo, A.P., 1998. Task 3 Define the conditions to be reproduced in the standard test –To develop a European standard dynamic water tightness test for curtain walling. Build. Res. Establ.

Pearson, K., 1900. X. On the criterion that a given system of deviations from the probable in the case of a correlated system of variables is such that it can be reasonably supposed to have arisen from random sampling. London, Edinburgh, Dublin Philos. Mag. J. Sci. 50, 157–175. https://doi.org/10.1080/14786440009463897.

Pérez-Bella, J.M., Domínguez-Hernández, J., Rodríguez-Soria, B., del Coz-Díaz, J.J., Cano-Suñén, E., 2013. Combined use of wind-driven rain and wind pressure to define water penetration risk into building façades: the Spanish case. Build. Environ. 64, 46–56. https://doi.org/10.1016/j.buildenv.2013.03.004.

Rousseau, M., 1999. Overview of the survey of building envelope failures in the coastal climate of British Columbia, performed by Morrisson-Hershfield Limited for CMHC (1996). J. Therm. Envelope Build. Sci. 22, 364–367. https://doi.org/10.1177/109719639902200411.

Sacré, C., 1984. Concomitance de la plui et du vent en France: approche statistique. In: Colloque de Centre Scientifique et Technique Du Bâtiment: Étanchéité à l'eau Des Couvertures et Petits Éléments Sous l'effet de La Concomitance Vent-Plui, pp. 18–21.

Sahal, N., Lacasse, M.A., 2005. Water entry function of a hardboard siding-clad wood stud wall. Build. Environ. 40, 1479–1491. https://doi.org/10.1016/j.buildenv.2004.11.019.

Sahal, N., Lacasse, M.A., 2004. Experimental Assessment of Water Penetration and Entry into Siding-Clad Wall Specimen. NRC Publications Archive. https://doi.org/10.4224/20377802.

Schwarz, G., 1978. Estimating the dimension of a model. Ann. Stat. 6, 461–464. https://doi.org/10.1214/aos/1176344136.

Sherman, C.W., 1931. Frequency and intensity of excessive rainfalls at boston, Massachusetts. Trans. Am. Soc. Civ. Eng. 95, 951–960. https://doi.org/10.1061/TACEAT.0004286.

Smegal, J., Lstiburek, J., Straube, J., Grin, A., 2013. Moisture-related durability of walls with exterior insulation in the pacific northwest. In: Thermal Performance of the Exterior Envelopes of Whole Buildings - 12th International Conference. American Society of Heating, Refrigeration, and Air-Conditioning Engineers (ASHRAE).

Straube, J.F., Burnett, E.F.P., 2000. Simplified prediction of driving rain on buildings. In: Proceedings of the International Building Physics Conference, pp. 375–382.

Surry, D., Skerlj, P., Mikitiuk, M., 1997. An exploratory study of the climatic relationships between rain and wind. J. Therm. Insul. Build. Envelopes 21, 121–124. https://doi.org/10.1177/109719639702100202.

Tang, W., Davidson, C.I., Finger, S., Vance, K., 2004. Erosion of limestone building surfaces caused by wind-driven rain: 1. Field measurements. Atmos. Environ. 38, 5589–5599. https://doi.org/10.1016/j.atmosenv.2004.06.030.

Van Balen, K., 1996. Expert system for evaluation of deterioration of ancient brick masonry structures. Sci. Total Environ. 189– 190, 247–254. https://doi.org/10.1016/0048-9697(96)05215-1.

Van Den Bossche, N., Lacasse, M.A., Janssens, A., 2013. A uniform methodology to establish test parameters for watertightness testing part II: Pareto front analysis on co-occurring rain and wind. Build. Environ. 63, 157–167. https://doi.org/10.1016/j.buildenv.2012.12.019.

Wang, X.J., Li, Q.S., Li, J.C., 2020. Field measurements and numerical simulations of wind-driven rain on a low-rise building during typhoons. J. Wind Eng. Ind. Aerod. 204, 104274. https://doi.org/10.1016/j.jweia.2020.104274.